Article

Cell Reports

Gut Microbiota Modulate CD8 T Cell Responses to Influence Colitis-Associated Tumorigenesis

Graphical Abstract

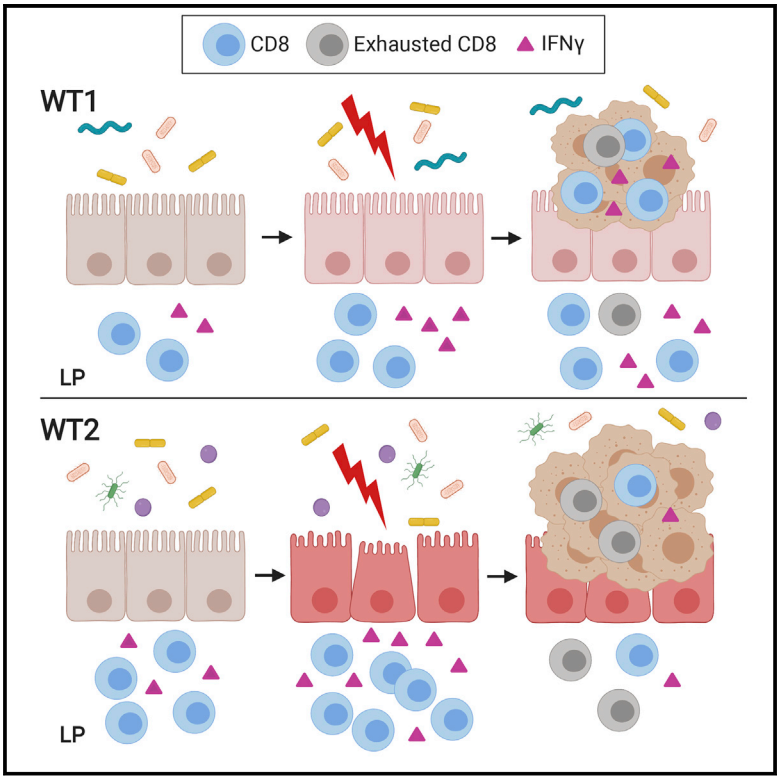

Authors

Amy I. Yu, Lili Zhao, Kathryn A. Eaton, ..., Patrick D. Schloss, Eric C. Martens, Grace Y. Chen

Correspondence

gchenry@umich.edu

In Brief

The gut microbiome is capable of modulating intestinal inflammation and tumorigenesis. Yu et al. demonstrate that dysbiosis can lead to increased susceptibility to inflammation-associated colon tumorigenesis via the induction of pro-inflammatory $CD8^+$ $IFN\gamma^+$ T cells, which can lead to increased T cell exhaustion within the tumor microenvironment.

Highlights

- Dysbiosis can lead to increased colon tumor susceptibility and $CD8^+$ $IFN\gamma^+$ T cells
- Increased colon $CD8^+$ $IFN\gamma^+$ T cells are associated with more inflammation and tumors
- Dysbiosis and increased tumorigenesis are associated with greater T cell exhaustion

Yu et al., 2020, Cell Reports *31*, 107471
April 7, 2020
https://doi.org/10.1016/j.celrep.2020.03.035

CellPress

Cell Reports
Article

Gut Microbiota Modulate CD8 T Cell Responses to Influence Colitis-Associated Tumorigenesis

Amy I. Yu,[1] Lili Zhao,[2] Kathryn A. Eaton,[3] Sharon Ho,[4] Jiachen Chen,[5] Sara Poe,[6] James Becker,[6] Allison Gonzalez,[4] Delaney McKinstry,[4] Muneer Hasso,[4] Jonny Mendoza-Castrejon,[7] Joel Whitfield,[8] Charles Koumpouras,[3] Patrick D. Schloss,[3] Eric C. Martens,[3] and Grace Y. Chen[1,5,9,*]

[1]Graduate Program in Immunology, University of Michigan, Ann Arbor, MI 48109, USA
[2]Department of Biostatistics, University of Michigan, University of Michigan, Ann Arbor, MI 48109, USA
[3]Department of Microbiology and Immunology, University of Michigan, Ann Arbor, MI 48109, USA
[4]College of Literature, Science, and the Arts, University of Michigan, Ann Arbor, MI 48109, USA
[5]Department of Internal Medicine, University of Michigan, Ann Arbor, MI 48109, USA
[6]Unit for Laboratory Animal Medicine, University of Michigan, Ann Arbor, MI 48109, USA
[7]Postbac Research Education Program, University of Michigan, Ann Arbor, MI 48109, USA
[8]Cancer Center Immunology Core, University of Michigan, Ann Arbor, MI 48109, USA
[9]Lead Contact
*Correspondence: gchenry@umich.edu
https://doi.org/10.1016/j.celrep.2020.03.035

SUMMARY

There is increasing evidence that gut microbiome perturbations, also known as dysbiosis, can influence colorectal cancer development. To understand the mechanisms by which the gut microbiome modulates cancer susceptibility, we examine two wild-type mouse colonies with distinct gut microbial communities that develop significantly different tumor numbers using a mouse model of inflammation-associated tumorigenesis. We demonstrate that adaptive immune cells contribute to the different tumor susceptibilities associated with the two microbial communities. Mice that develop more tumors have increased colon lamina propria CD8$^+$ IFNγ^+ T cells before tumorigenesis but reduced CD8$^+$ IFNγ^+ T cells in tumors and adjacent tissues compared with mice that develop fewer tumors. Notably, intratumoral T cells in mice that develop more tumors exhibit increased exhaustion. Thus, these studies suggest that microbial dysbiosis can contribute to colon tumor susceptibility by hyperstimulating CD8 T cells to promote chronic inflammation and early T cell exhaustion, which can reduce anti-tumor immunity.

INTRODUCTION

Colorectal cancer (CRC) is the third most common cause of cancer and fourth leading cause of cancer-related deaths worldwide (Arnold et al., 2017). In addition to the presence of specific gene mutations, host immune responses significantly contribute to the development and progression of CRC (Markman and Shiao, 2015). For example, chronic inflammation results in the production of DNA-damaging reactive oxygen species and pro-inflammatory mediators that promote cellular survival and growth. Consequently, patients with inflammatory bowel disease (IBD) are at increased risk for developing CRC (Eaden et al., 2001). Host immunity also contributes to immune surveillance and anti-tumor activity (Markman and Shiao, 2015; Pernot et al., 2014). Consistently, tumors with higher densities of effector CD8 T cells and a Th1 gene signature are associated with better prognosis (Galon et al., 2006). Thus, factors that influence the balance of these processes likely affect CRC risk.

The gut microbiome is recognized as having a role in modulating both host immunity and susceptibility to colon tumorigenesis. For example, the gut microbiota can influence frequencies of intestinal lamina propria (LP) immune cells, notably regulatory T cells (Tregs) and T helper 17 (Th17) cells (Atarashi et al., 2011; Furusawa et al., 2013; Geva-Zatorsky et al., 2017) which can affect inflammatory responses and tumor susceptibility (Műzes et al., 2012; Razi et al., 2019; Wu et al., 2009). Certain human gut bacteria can promote IFNγ production by CD8 T cells and anti-tumor immunity in mice (Tanoue et al., 2019). How these immunomodulatory activities ultimately contribute to CRC susceptibility remains to be fully elucidated.

CRC patients exhibit altered gut microbiomes typically characterized by decreased *Firmicutes* and increased *Bacteroidetes* bacteria compared with healthy controls (Ahn et al., 2013; Baxter et al., 2014; Wang et al., 2012; Zackular et al., 2014). Specific bacteria have consistently been enriched in colon tumors, such as *Escherichia coli* positive for the polyketide synthase (pks) pathogenicity island, enterotoxigenic *Bacteroides fragilis* (ETBF), and *Fusobacterium nucleatum*. Some proposed mechanisms, largely based on mice studies, include the promotion of DNA damage (Arthur et al., 2012; Nougayrède et al., 2006), the induction of pro-inflammatory Th17 responses (Wu et al., 2009), and the inhibition of tumor-infiltrating lymphocytes (Gur et al., 2015). However, these bacteria are not associated with all CRC cases, and therefore, other bacterial populations likely contribute to tumor susceptibility via other mechanisms. Nonetheless, additional studies are needed to understand the

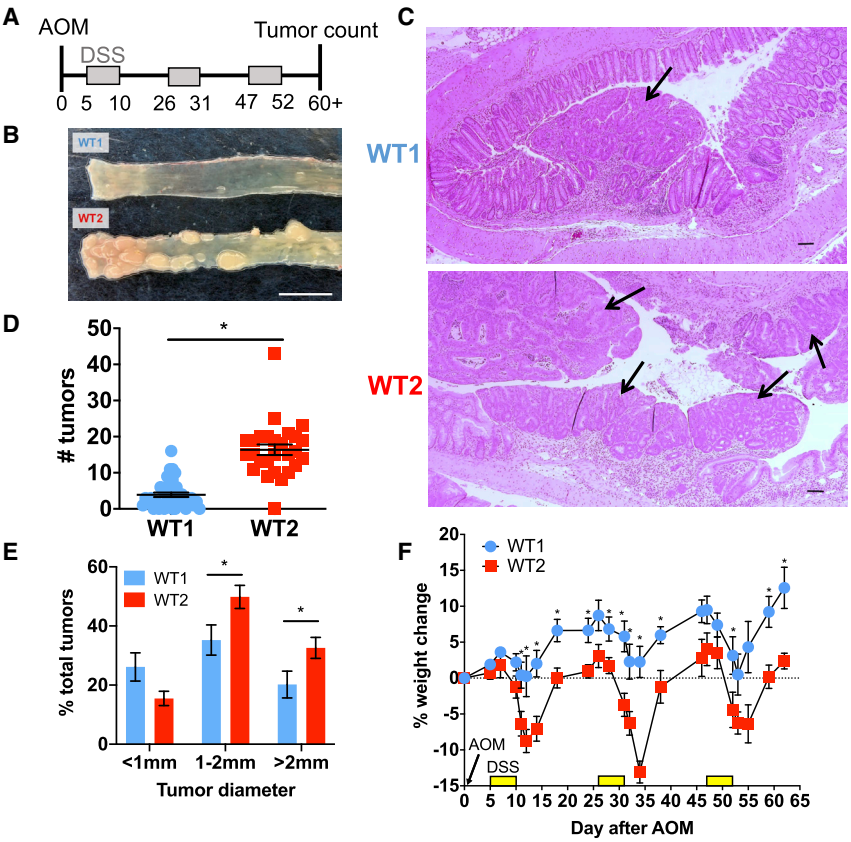

Figure 1. Two Colonies of C57BL/6J WT Mice Have Different Colon Tumor Burdens in the AOM/DSS Model of Inflammation-Associated Colon Tumorigenesis

(A) Schema of AOM/DSS model.

(B) Representative photo of WT1 and WT2 tumors. Scale bar, 1 cm.

(C) Representative micrographs of H&E stains of colon tissue at the tumor endpoint at 40× magnification. Tumors are denoted by black arrows. Scale bar, 100 μm.

(D and E) Tumor numbers (D) and sizes (E) are shown. WT1, n = 42; WT2, n = 36.

(F) Representative graph of percentage weight change during AOM/DSS treatment compared with day 0. n = 5 mice/group.

Data are mean ± SEM and are representative of or pooled from at least three experiments. *p < 0.05 by Mann-Whitney test.

See also Figure S1.

mechanisms by which perturbations in the gut microbiome, also known as dysbiosis, affect colon tumorigenesis.

In this study, we take advantage of the different susceptibilities of two wild-type (WT) C57BL/6J mouse colonies in our facility and use a mouse model of inflammation-associated tumorigenesis to identify factors that contribute to increased inflammation and colon tumorigenesis. Specifically, mice from our "WT1" colony developed an average of 5 tumors, and mice from our "WT2" colony developed an average of 15 tumors. Sequencing of fecal bacteria from WT1 and WT2 mice indicate that the two colonies have distinct microbiomes, which when transferred into germ-free (GF) WT mice recapitulated their respective tumor susceptibilities. Interestingly, cohousing and cross-fostering studies resulted in intermediate tumor phenotypes with hybrid microbiomes. By cross-referencing microbiome compositions after microbiome transfer with tumor outcomes, we identified candidate bacteria consistently associated with low or high tumor burdens. Additionally, naive and acutely inflamed WT2 mice have increased colon LP $CD8^+$ $IFN\gamma^+$ T cells compared with WT1 mice. However, after tumor development, WT2 mice exhibited decreased intratumoral $CD8^+$ $IFN\gamma^+$ T cell numbers and increased CD8 T cell exhaustion. Both GF *Rag1*$^{-/-}$ and specific pathogen-free (SPF) *Cd8*$^{-/-}$ mice colonized with WT2 microbiota resulted in fewer tumor numbers than SPF WT2 mice. These results strongly suggest that CD8 T cells may play a pro-inflammatory and pro-tumorigenic role in the context of a dysbiotic microbiome and that dysbiosis can contribute to increased tumor susceptibility by increasing T cell exhaustion.

RESULTS

Differences in Gut Microbiome Composition Directly Contribute to Inflammation-Associated Tumor Susceptibility

We have previously demonstrated that alterations in the gut microbiome can directly contribute to tumorigenesis (Zackular et al., 2013). In this study, we used the azoxymethane (AOM)/dextran sulfate sodium (DSS) model of inflammation-associated colon tumorigenesis (De Robertis et al., 2011; Tanaka et al., 2003), in which mice are given an intraperitoneal injection of the carcinogen AOM followed by three rounds of water containing 2% DSS, which compromises the intestinal barrier, resulting in increased epithelial permeabilization and inflammation (Chassaing et al., 2014). In this model, tumors develop by weeks 8–10 (Neufert et al., 2007; Zackular et al., 2013) (Figure 1A). Although this model is driven by epithelial injury and inflammation and has been used to understand the pathogenesis of IBD-associated CRC, there are features of this model that also recapitulate sporadic CRC, including the predominance of tumor mutations that dysregulate Wnt signaling (Greten et al., 2004; Zhan et al., 2013), which occurs in the majority of human CRC, as well as the progression from adenomas to adenocarcinomas (Suzuki et al., 2004). AOM/DSS treatment also results in microbiome alterations similar to that observed in human CRC patients such as reduced species richness and alpha diversity as well as significant shifts in beta diversity (Zackular et al., 2013).

In our previous study (Zackular et al., 2013), we observed C57BL/6 (B6) WT mice with higher tumor numbers after AOM/DSS treatment than what we have typically observed (Chen et al., 2008; Zhan et al., 2016). Specifically, when we compared the two mouse colonies, "WT1" mice developed 5 tumors on average, whereas "WT2" mice developed 15 tumors on average (Figures 1B–1D). WT2 mice not only developed larger tumors but

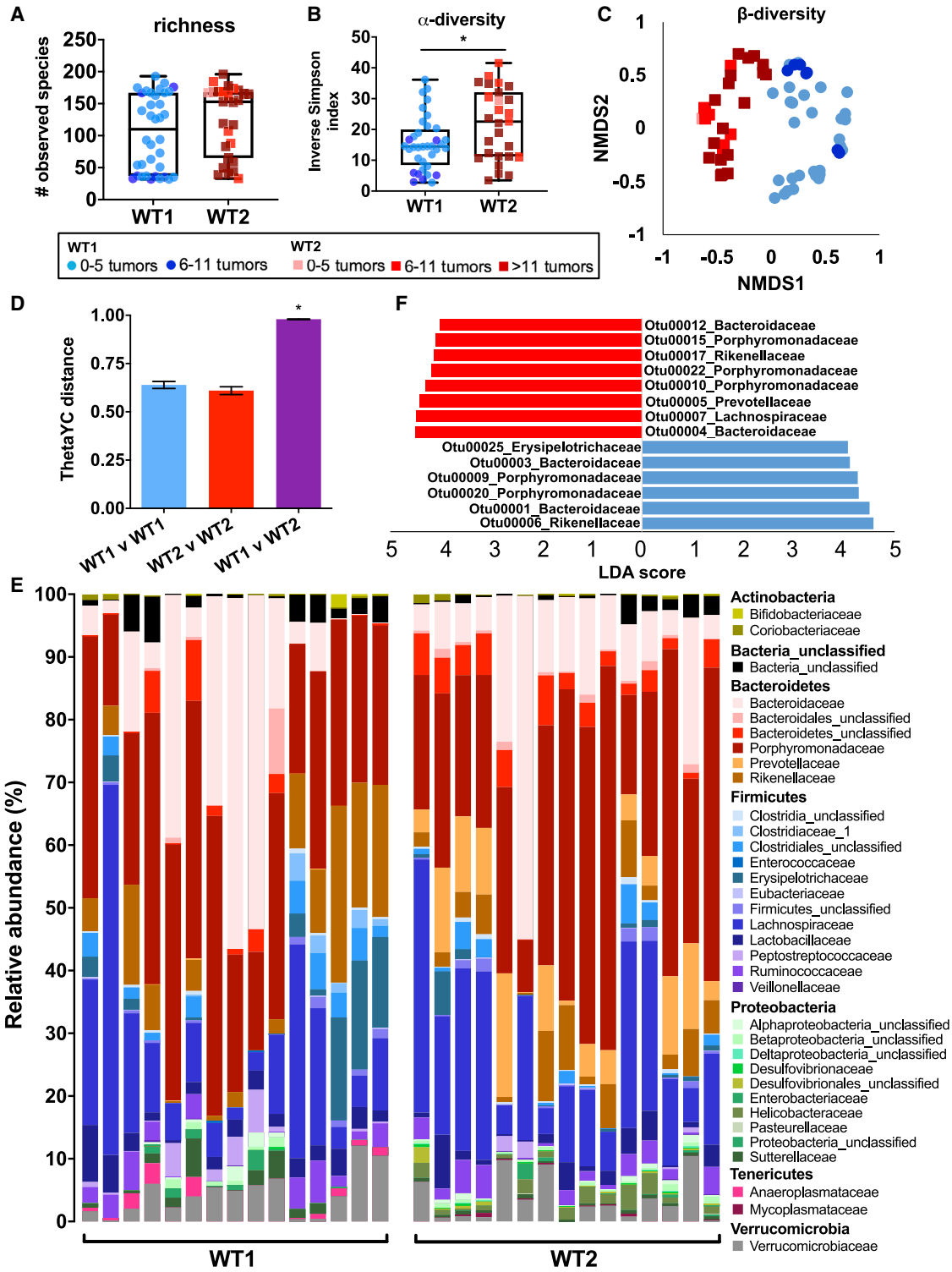

Figure 2. Gut Microbiome Compositions in WT1 and WT2 Mice Are Significantly Different

(A–C) 16S rRNA sequencing of naive WT1 and WT2 fecal microbiota was performed, and richness (A) and alpha diversity (B) were measured. Beta diversity (C) is shown as a nonmetric dimensional scaling (NMDS) plot. *$p < 0.05$ by Mann-Whitney test.

(D) Microbiome composition dissimilarity based on thetaYC distances. *$p < 0.05$ by AMOVA.

(legend continued on next page)

also exhibited increased weight loss after DSS treatment compared with WT1 mice (Figures 1E and 1F). Additionally, during the acute inflammatory response to the first round of DSS (day 12), WT2 mice have significantly more colonic inflammation on the basis of levels of stool lipocalin-2, a surrogate marker for intestinal inflammation (Chassaing et al., 2012), and histologic scoring (Figures S1A and S1B).

Although both WT1 and WT2 colonies originate from Jackson B6 mice and are housed in the same mouse room, WT2 mice were generated during backcrossing of WT1 mice with a transgenic knockout (KO) mouse strain that exhibited increased tumor susceptibility after AOM/DSS treatment (Chen et al., 2008) and were also housed on the same rack as the KO strain. We therefore hypothesized that dysbiotic microbiota from the KO strain were transferred to WT2 mice, resulting in similarly increased susceptibility to colon tumorigenesis. To examine microbiome differences between the two colonies, we performed 16S rRNA sequencing on stool-extracted DNA from untreated WT1 and WT2 mice. Although no difference in species richness was measured between the gut microbiomes of the two colonies, WT2 microbiomes had increased alpha diversity compared with WT1 microbiomes (Figures 2A and 2B). Beta diversity was visualized by nonmetric multidimensional scaling (NMDS) ordination, which showed two separate clusters representing the microbiomes of WT1 and WT2 mice, suggesting that WT1 and WT2 colonies have distinct microbiome compositions (Figure 2C). Consistently, the gut microbial community structures of WT1 and WT2 mice were significantly dissimilar, as determined by θ_{YC} (thetaYC) distances and analysis of molecular variance (AMOVA) (Figure 2D).

WT1 and WT2 microbiomes are differentially abundant in certain bacteria families. WT1 mice have increased *Anaeroplasmataceae*, *Erysipelotrichaceae*, *Clostridiales*, and *Sutterellaceae* bacteria, while WT2 mice have increased *Prevotellaceae* and *Helicobacteraceae* bacteria (Figure 2E). To identify specific differences between the two microbiomes, we used linear discriminant analysis (LDA) effect size (LEfSe) analysis (Segata et al., 2011) to identify operational taxonomic units (OTUs), which are bacterial sequences that are at least 97% identical, significantly associated with WT1 or WT2 microbiomes (Figure 2F). Consistent with the relative abundance data, among the most differentially significant OTUs, WT1 mice are enriched in a member of the *Erysipelotrichaceae* family, and WT2 mice are enriched in a member of the *Prevotellaceae* family, which has also been observed in human CRC patients (Sobhani et al., 2011; Wang et al., 2012).

To determine whether the microbiome differences between WT1 and WT2 colonies are directly responsible for the differences in tumor phenotype, we gavaged anaerobically prepared stool and cecal homogenates of SPF WT1 or WT2 mice into GF WT mice. Additionally, to determine whether cultivable bacteria from WT1 or WT2 microbiomes also contribute to tumor susceptibility, stool and cecal homogenates were plated onto specific media plates and anaerobically cultured. Bacterial colonies were resuspended in anaerobic PBS and gavaged into GF WT mice. After 4 weeks of colonization, GF WT mice had stool bacteria levels comparable with those of SPF mice as measured by qPCR using universal bacteria primers (data not shown), and their microbiomes also recapitulated the donor or input composition by thetaYC measurement (Figures S2A and S2B). After AOM/DSS treatment, GF WT mice with WT1 bacteria (SPF WT1 > GF) developed significantly fewer and smaller tumors compared with GF WT mice with WT2 bacteria (SPF WT2 > GF), suggesting that microbiome differences directly promote tumor burden differences (Figures 3A–3C). Interestingly, GF WT mice gavaged with cultivable WT2 bacteria (cult WT2 > GF) also developed more tumors compared with GF WT mice gavaged with cultivable WT1 bacteria (cult WT1 > GF) but developed significantly fewer and smaller tumors compared with SPF WT2 > GF (Figures 3A–3C). These data suggest that the different tumor susceptibilities of WT1 and WT2 mice can be attributed to gut microbiome differences and that the absence or presence of specific bacterial populations, some of which may be cultivable, can determine tumor outcomes.

Cohousing and Cross-Fostering Are Insufficient to Completely Transfer Microbiomes and Are Associated with Intermediate Phenotype Transmission

We next wanted to examine if the tumor burden phenotype could be transferred between WT1 and WT2 mice via cohousing, which has been commonly used to transmit microbiome-dependent phenotypes. Age-matched female WT1 and WT2 mice were first mostly cohoused in a 2:2 ratio for 4 weeks before AOM/DSS treatment (Figure 4A, "coh"). Cohoused WT1 and WT2 mice exhibited significant tumor burden differences similar to non-cohoused control mice (Figure 4B, "coh"). Although the microbiota of cohoused WT1 and WT2 mice were not significantly different from each other after 4 weeks of cohousing on the basis of thetaYC distances, cohoused WT1 microbiome compositions remained significantly different from control WT2 microbiomes (Figure S2C). Cohoused WT2 microbiomes also remained distinct from control WT1 microbiomes on the basis of thetaYC measurements, suggesting incomplete microbiome transfer (Figure S2C). Additionally, by NMDS ordination, cohoused WT1 and cohoused WT2 mice cluster separately (Figure S2D).

Although cohousing did not result in complete transmission of tumor phenotype from either WT1 or WT2 mice to the other, two cohoused mice developed tumors similar in number to mice from the other colony (Figure 4B, black boxes). These mice were cohoused in a 1:1 ratio (one WT1 and one WT2 mouse), which may have resulted in more efficient microbiome transfer by coprophagy. We therefore performed one-to-one (oto) cohousing experiments and also extended the cohousing time to 6 weeks to improve microbiome and phenotype transmission. However, significant tumor burden differences were

(E) Relative bacteria family abundances of naive WT1 and WT2 mice. n = 15/group

(F) The most differentially abundant OTUs between WT1 (blue) or WT2 (red) microbiomes were determined using LEfSe pairwise analysis. OTUs with LDA scores greater than 4 are shown.

Data are pooled from at least five experiments; WT1, n = 51; WT2, n = 45, unless otherwise noted.

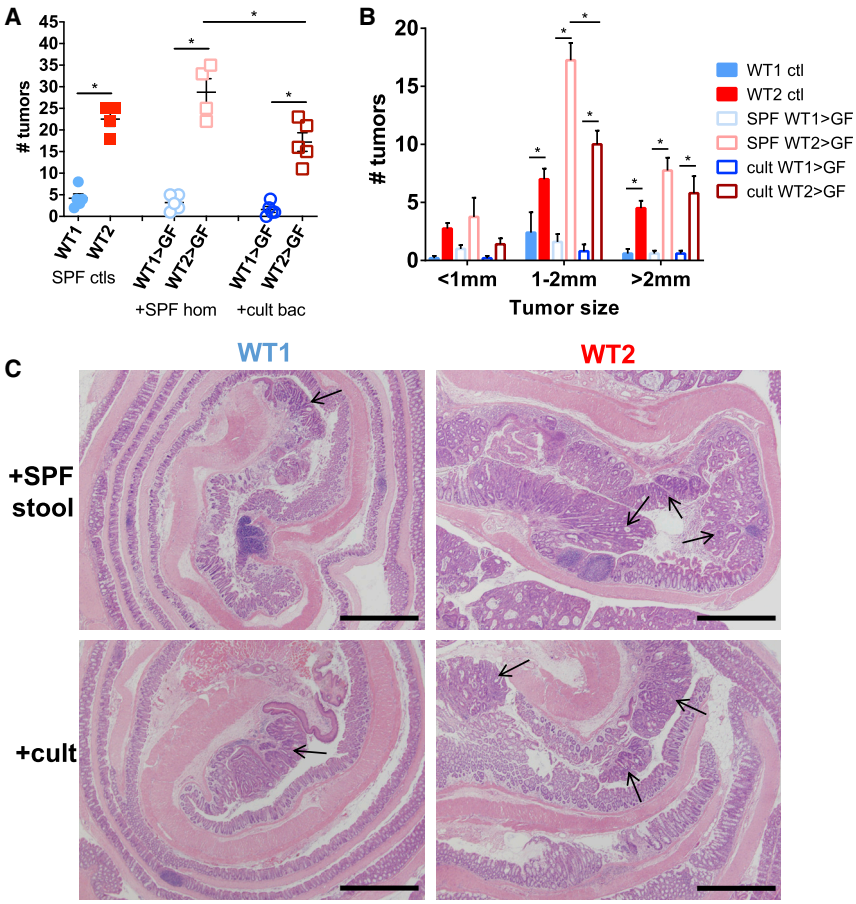

Figure 3. The Gut Microbiomes of WT1 and WT2 Mice Directly Contribute to Tumor Susceptibility

(A and B) Tumor number (A) and sizes (B) of AOM/DSS-treated GF WT mice that were colonized with SPF WT1 or WT2 whole-stool and cecal homogenates or anaerobically cultivable WT1 or WT2 stool and cecal bacteria for 4 weeks. Tumors were counted 10 days after the last DSS round. Data are mean ± SEM. n = 4 or 5/group. *p < 0.05 by Mann-Whitney test.

(C) Representative micrographs of H&E stains of colon tissue at the tumor endpoint at 40× magnification. Tumors are denoted by black arrows. Scale bar, 1 mm.

See also Figure S2.

still observed between oto cohoused WT1 and WT2 mice (Figure 4B, "oto"). Furthermore, oto cohoused WT2 mice developed an intermediate tumor burden phenotype, and no differences in tumor number between oto cohoused and control WT1 mice were measured (Figure 4B, "oto"). With regard to microbiome composition, oto cohoused WT2 mice were significantly different from WT1 controls, again suggesting incomplete microbiome transfer despite oto cohousing (Figure S2E). By NMDS ordination, microbiome compositions of oto cohoused WT1 and WT2 mice clustered between control WT1 and WT2 mice, suggesting that oto cohoused mice have a hybrid microbiome, which may explain the intermediate tumor phenotype (Figure S2F).

As the gut microbiome of an adult mouse is typically determined by maternal transmission, cross-fostering is another microbiome transfer method and may be more effective than cohousing (Daft et al., 2015; Moore and Stanley, 2016). We performed cross-fostering experiments in which WT1 or WT2 pups were switched within 48 h of birth to a WT2 or WT1 nursing mother, respectively. Cross-fostered mice were treated with AOM/DSS after reaching 6 weeks of age. Unlike with cohousing, cross-fostered WT1 and WT2 mice no longer developed significantly different tumor burdens; however, average tumor numbers were again intermediate between control WT1 and WT2 mice (Figure 4B, "CF"). When we examined gut microbiome compositions of cross-fostered mice, we determined that the microbial community of WT1 mice cross-fostered by WT2 nursing mothers (WT1[WT2]) and WT2 mice cross-fostered by WT1 nursing mothers (WT2[WT1]) remained distinct (Figure S2G). Although microbiomes of WT2(WT1) and non-cross-fostered WT1 mice were overall similar, the microbiome compositions of WT1(WT2) and non-cross-fostered WT2 mice were still significantly different despite improved microbiome transfer compared with cohousing on the basis of thetaYC and NMDS ordination (Figures S2G and S2H). There were also significant differences in specific bacterial populations between WT1(WT2) or WT2(WT1) mice and WT2 or WT1 mice by LEfSe (data not shown), respectively, which may explain why the tumor phenotype was not fully transmissible.

Specific Bacteria Are Associated with Low or High Tumor Burdens

As we observed multiple tumor phenotypes associated with various microbial communities that were generated from different microbiome transfer methods, we reasoned that certain bacterial populations may consistently be associated with either low or high tumor burdens regardless of WT colony origin. We therefore examined 16S rRNA sequences from the stool of cohoused and cross-fostered WT1 and WT2, control WT1 and WT2 mice, and GF WT mice conventionalized with WT1 or WT2 microbiota that was collected just prior to AOM/DSS treatment to identify OTUs that directly correlated with tumor outcomes after AOM/DSS treatment. On the basis of relative abundances alone, we observed, for example, increased abundance of *Prevotellaceae* in day 0 mice that developed high tumor numbers and increased abundance of *Anaeroplasmataceae* in mice that developed low tumor burdens (Figure S2I). OTUs that were significantly associated with low or high tumor numbers were determined by the combination of the following analyses: Metastats (White et al., 2009), LEfSe (Segata et al.,

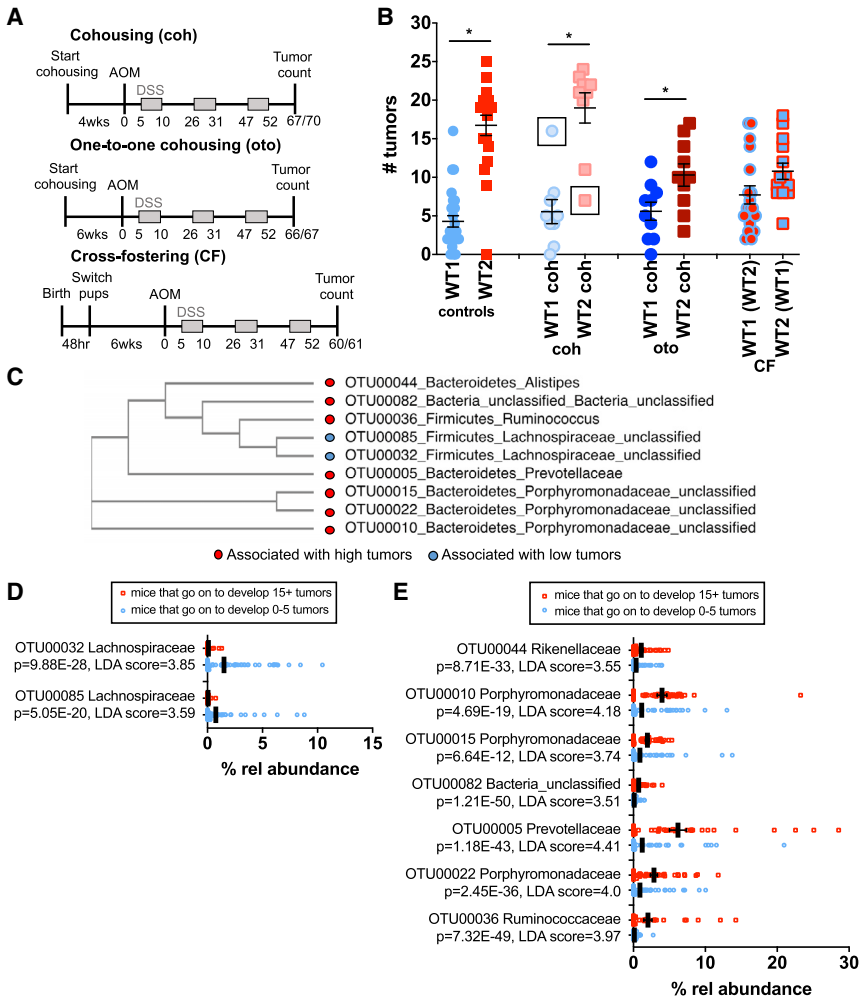

Figure 4. Specific Bacterial Populations Correlate with High or Low Tumor Susceptibilities

(A) WT1 and WT2 mice were cohoused in a 2:2 ratio (coh) for 4 weeks or a 1:1 ratio (oto) for 6 weeks or cross-fostered (CF). Mice were treated with AOM/DSS and sacrificed for tumor counting on days 60–70 depending on the experiment.

(B) Number of tumors in indicated mice after AOM/DSS treatment. The control group includes pooled control mice from all cohousing and cross-fostering experiments. Data are mean ± SEM; controls: WT1, n = 27; WT2, n = 20; coh: n = 9/group; oto: n = 10/group; CF: WT1(WT2), n = 18; WT2(WT1), n = 14. *$p < 0.05$ by Mann-Whitney test.

(C) Phylogenetic tree of nine bacterial candidates associated with low (blue) or high (red) tumor burdens on the basis of sequence similarity.

(D and E) Relative bacterial abundances in mice at the time of AOM injection that were associated with low (D) or high (E) tumor burdens. Black lines denote mean relative abundances. Poisson regression p values are shown. LDA scores were determined using LEfSe analyses. Low, n = 85; high, n = 38.

Data shown are pooled from at least two independent experiments per microbiome transfer method.

See also Figure S2.

Dysbiotic Microbiome from WT2 Mice Promotes Inflammation-Associated Tumorigenesis via Adaptive Immune Cells

An important characteristic of the gut microbiota is its ability to modulate host immune responses (Belkaid and Hand, 2014; Geva-Zatorsky et al., 2017). To determine whether the difference in tumor susceptibilities between WT1 and WT2 mice were associated with altered baseline immune responses, LP immune cell compositions from the entire colon of untreated WT1 and WT2 mice were analyzed using flow cytometry. No differences in colon LP monocytes, neutrophils, dendritic cells (DCs), or natural killer (NK) cells were observed; however, WT2 mice have increased B and T cell populations compared with WT1 mice, suggesting that the WT2 microbiome may exert its tumor-promoting effect via adaptive immune cells (Figure 5A).

To examine this possibility, GF *Rag1*$^{-/-}$ mice were colonized with SPF WT1 or WT2 stool and cecal homogenates, which resulted in successful colonization of WT1 and WT2 microbiomes after 4 weeks (Figures S3A and S3B). After induction of tumors by AOM/DSS, GF *Rag1*$^{-/-}$ mice with WT2 microbiota developed fewer and smaller tumors compared with SPF WT2 controls (Figures 5C and 5D), suggesting that the dysbiotic WT2 microbiome promotes tumor susceptibility by acting on adaptive immune cells. GF *Rag1*$^{-/-}$ mice with WT1 microbiota developed slightly increased tumor numbers compared with SPF WT1 control mice (Figure 5C), which may indicate a protective role for adaptive immune cells in the context of the WT1 microbiome. Of note,

2011), random forest (Zackular et al., 2015), and linear and Poisson regression. In particular, we identified nine OTUs belonging to at least five different bacterial families that were significantly associated with either low or high tumor numbers (Figure 4C). Many of these bacteria have not been previously classified, but phylogenetic tree analysis on the basis of 16S sequence similarity suggests that some of the bacteria within a family may be closely related (Figure 4C) (Clarridge, 2004; Edgar, 2018).

Specifically, two OTUs from the *Lachnospiraceae* family are significantly associated and predictive of low tumor burdens. These OTUs are also more abundant in mice that eventually developed low tumor numbers (Figure 4D). On the other hand, seven OTUs, including bacteria in the *Prevotellaceae* family, are predictive of high tumor burdens and are more abundant in mice that develop high tumor numbers (Figures 2E, 4E, and S2I). Of note, although *Helicobacteraceae* appeared to be more abundant in WT2 mice (Figure 2E), it was not significantly associated with tumor numbers by linear regression or Metastats analyses. Altogether, these data reveal nine bacterial populations that may have tumor-suppressive or tumor-promoting activities.

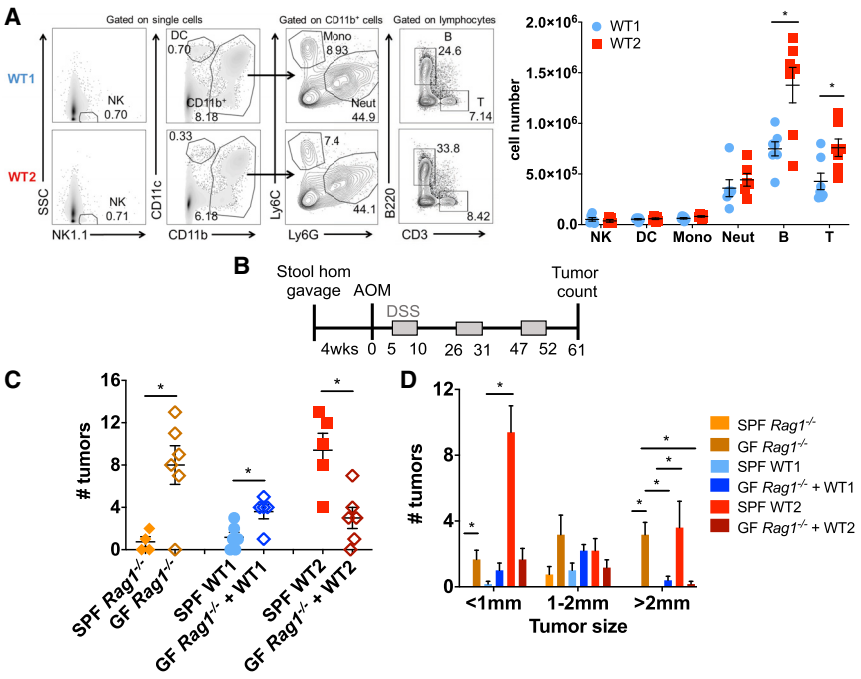

Figure 5. Adaptive Immune Cells Contribute to Increased Tumor Susceptibility of WT2 Mice

(A) Colon LP immune cells from untreated WT1 and WT2 mice were analyzed using flow cytometry. Data are pooled from at least two independent experiments. n = 5–7/group.

(B) GF *Rag1*$^{-/-}$ mice were gavaged with SPF WT1 or WT2 stool and cecal contents followed by AOM/DSS treatment after 4 weeks of colonization. Mice were sacrificed on day 61 for tumor counting.

(C and D) Tumor number (C) and sizes (D) are shown. n = 4–6/group.

Data are mean ± SEM. *p < 0.05 by Mann-Whitney test.

See also Figure S3.

GF *Rag1*$^{-/-}$ had significantly higher tumor numbers compared with that of SPF *Rag1*$^{-/-}$, which is consistent with previous reports demonstrating increased susceptibility of GF mice to DSS-induced injury and AOM/DSS-induced tumorigenesis (Maslowski et al., 2009; Zhan et al., 2013)

Naive WT2 Mice that Have Increased Tumor Susceptibility Have Increased IFNγ-Producing CD8 T Cells in the Colon LP

We and others have previously shown a role of T cells in affecting tumor susceptibility in the AOM/DSS model (Becker et al., 2004; Zhan et al., 2016). To determine if T cell activity was altered between WT1 and WT2 mice, we examined LP T cell cytokine production after *ex vivo* stimulation by phorbol myristate cetate (PMA) and ionomycin. Specifically, colon LP CD8$^+$, but not CD4$^+$, IFNγ$^+$ T cells were increased in naive WT2 mice (Figures 6A and 6B), which was not observed in the mesenteric lymph nodes (Figures S4A–S4C). In contrast, there were no differences in colon LP CD4$^+$ IL-17$^+$ or CD4$^+$ Foxp3$^+$ cells (Figure 6B), suggesting that Th17 and Treg cells do not contribute to the increased inflammation and tumor susceptibility of WT2 mice. Furthermore, we measured increased activated CD8$^+$ CD69$^+$ cells, resident memory CD8$^+$ CD69$^+$ CD103$^+$ cells, and effector memory CD8$^+$ CD44$^+$ CD62L$^-$ cells in the colon LP of WT2 mice, whereas there were no differences in activated, resident memory, or effector memory CD4 T cells in the colon LP between WT1 and WT2 mice (Figures S4D–S4F).

We next analyzed the colon LP immune cell composition during the acute inflammatory response to DSS, specifically on day 12, when immune cell infiltration typically peaks (data not shown). As in naive mice, there were significantly increased CD3 and CD8, but not CD4, T cells in WT2 mice (Figures S4G and S4H). Additionally, colon LP CD8$^+$ IFNγ$^+$ T cells were increased in WT2 mice, but no differences in CD4$^+$ IFNγ$^+$, CD4$^+$ IL-17$^+$, or CD4$^+$ Foxp3$^+$ subsets were measured (Figure S4I). Colon LP monocytes and neutrophils were also elevated to a greater extent than in WT1 mice (Figure S4G), likely reflecting greater levels of inflammation in WT2 mice due to DSS treatment (Figure S1).

To determine whether CD8 T cells specifically contributed to increased tumorigenesis in WT2 mice, SPF *Cd8*$^{-/-}$ mice were treated with an antibiotic cocktail and antifungal water before gavage of SPF WT1 or WT2 stool and cecal contents for 3 consecutive days. Four weeks after the last gavage, mice were treated with AOM/DSS to induce tumors (Figure 6C). By NMDS ordination, *Cd8*$^{-/-}$ mice colonized with WT1 microbiota (WT1 > CD8 KO) clustered with WT1 control mice, and *Cd8*$^{-/-}$ mice colonized with WT2 microbiota (WT2 > CD8 KO) clustered with WT2 control mice, suggesting near complete microbiome transfer (Figures S3C and S3D). Importantly, WT1 > CD8 KO mice developed similar tumor numbers as WT1 control mice, whereas WT2 > CD8 KO mice developed significantly fewer and smaller tumors compared with WT2 control mice (Figures 6D and 6E), strongly suggesting that the dysbiotic WT2 microbiome mediates its tumor-promoting effects in part via pro-inflammatory CD8 T cells, although CD8-independent mechanisms likely also contribute.

To determine if WT2 microbiota directly contributed to the increased CD8$^+$ IFNγ$^+$ T cell numbers in naive WT2 mice, we gavaged WT2 mice stool and cecal homogenates into SPF WT1 mice after antibiotic and antifungal water treatment, as described in Figure 6C. After 9 weeks of recolonization, WT1 mice reconstituted with WT2 microbiota (WT1+WT2bac) had microbiomes closely resembling WT2 donor input as well as antibiotic-treated WT2 mice reconstituted with WT2 microbiota (WT2+WT2bac) by NMDS ordination, although there were still significant differences between groups on the basis of thetaYC distances (Figures S5A and S5B). Importantly, WT1+WT2bac mice had increased colon LP CD3 and CD8, but not CD4,

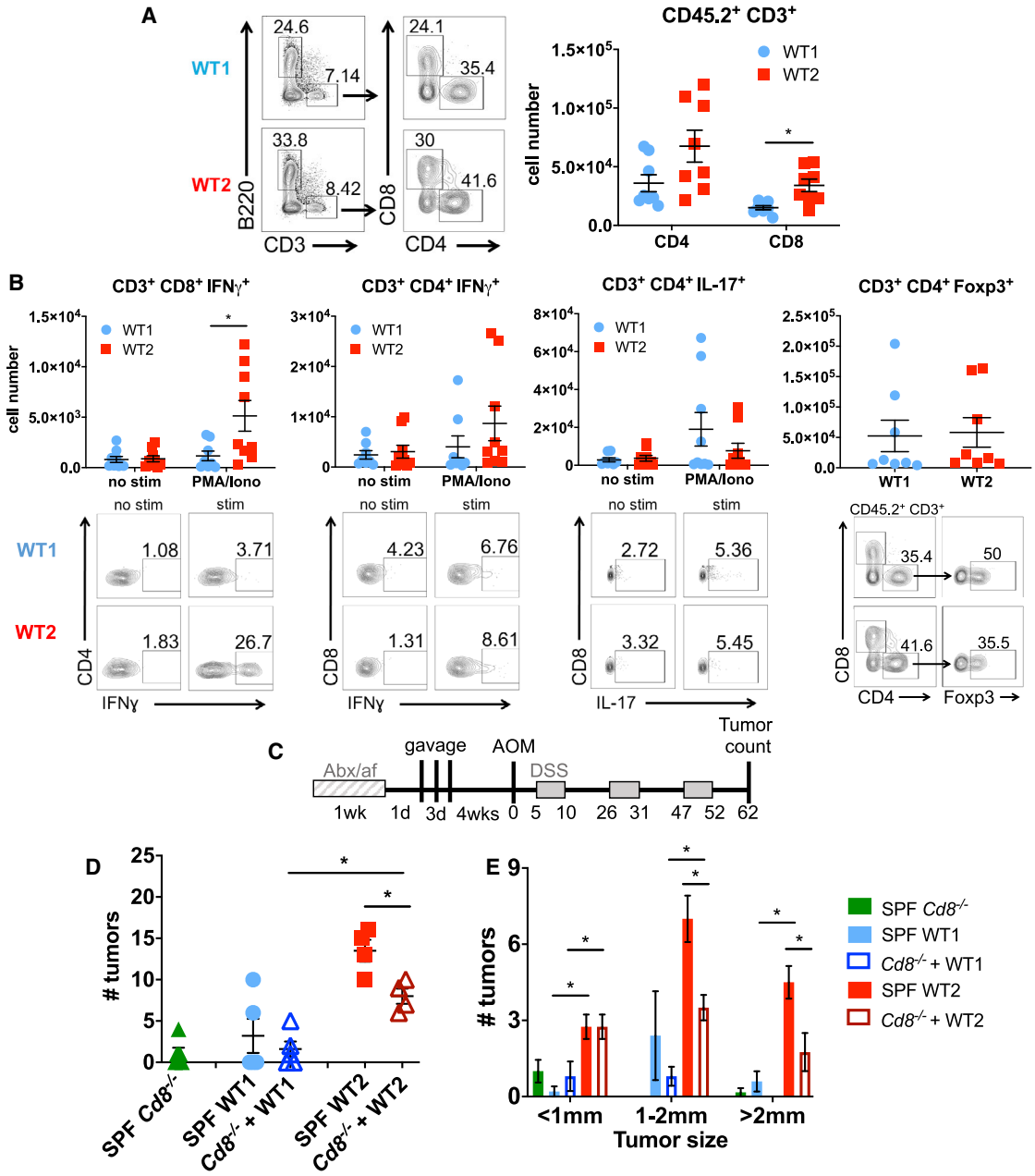

Figure 6. Naive WT2 Mice Exhibit Increased CD8$^+$ IFNγ T Cells in LP, which Partly Mediates Increased Tumor Susceptibility

(A) Numbers of CD4 and CD8 T cells in colon LP T cells of WT1 and WT2 mice as determined using flow cytometry. Data are pooled from at least two independent experiments. n = 8/group.

(B) Colon LP immune cells were *ex vivo*-stimulated with PMA and ionomycin with monensin for 4 h, and IFNγ, FoxP3, and IL-17 were measured using flow cytometry. Representative flow plots are shown. Data are pooled from at least two independent experiments. n = 8 or 9/group.

(C) SPF *Cd8*$^{-/-}$ mice were treated with antibiotics for 1 week prior to three consecutive gavages of SPF WT1 or WT2 microbiota followed by AOM and three rounds of 2% DSS after 4 weeks of bacteria colonization.

(D and E) Tumor number (D) and sizes (E) were measured on day 62 of AOM/DSS. n = 4–6/group.

Data are mean ± SEM. *p < 0.05 by Mann-Whitney test.

See also Figures S3–S7.

T cells, as well as increased CD8$^+$ IFNγ$^+$ T cells compared with the control WT1 mice that were recolonized with WT1 bacteria (WT1+WT1bac) (Figures S5C and S5D). WT1+WT2bac mice also had increased CD4$^+$ IFNγ$^+$ T cells, but no differences in CD4$^+$ IL-17$^+$ or CD4$^+$ Foxp3$^+$ subsets, compared with WT1+WT1bac mice (Figure S5D).

We also gavaged GF WT mice with SPF WT1 or WT2 microbiota as in Figure 3. After 8 weeks of colonization to allow microbial and immune cell reconstitution, colon LP immune cell populations were analyzed using flow cytometry. Although no differences in CD3, CD8, or CD4 T cells were observed (Figure S6A), GF WT mice colonized with WT2 microbiota had increased colon LP CD8$^+$ IFNγ^+ T cells, but no differences in CD4$^+$ IFNγ^+, CD4$^+$ IL-17$^+$ or CD4$^+$ Foxp3$^+$ subsets, similar to what is observed in naive SPF WT2 mice (Figure S6B).

To explore potential mechanisms of how the WT2 microbiome may alter CD8 T cell responses in the colons of WT2 mice, we examined the expression of the T cell chemoattractants CXCL9 and CXCL10 in the colon epithelium of naive WT1 and WT2 mice by qPCR, and observed no differences, suggesting that the increase in CD8 T cells in the colon LP of WT2 mice is not necessarily due to increased recruitment via epithelial chemokine production (Figure S7A). There were also no differences in the expression of IL-6 or the antimicrobial peptides Reg3γ and β-defensin2, which may predispose WT2 mice to inflammation (Figure S7A). Interestingly, in WT2 epithelium cells, there was increased IL-1β expression, which has been shown to promote effector T cell responses, including the production of IFNγ (Ben-Sasson et al., 2013), as well as occludin, although the significance of this is unclear. Production of IL-12 by DCs can also promote CD8 T cell activation and IFNγ production (Brzoza et al., 2004; Curtsinger et al., 1999; Trinchieri, 1998). To determine if WT2 bacteria promote increased IL-12 production by DCs, we cultured WT1 and WT2 bone marrow-derived DCs (BMDCs) with heat-killed (HK) stool microbiota from either WT1 or WT2 mice and measured IL-12 in the supernatant. HK WT2 microbiota promoted increased IL-12 production by both WT1 and WT2 BMDCs compared with HK WT1 microbiota (Figure S7B). Altogether, these data strongly support a role for the WT2 microbiota in upregulating colon LP IFNγ CD8 T cell responses.

Intratumoral T Cells in WT2 Mice Exhibit an Exhausted Phenotype with Decreased IFNγ Production

CD8 T cells and IFNγ production are important for anti-tumor immunity (Castro et al., 2018; Galon et al., 2006; Mager et al., 2016; Pagès et al., 2005); consistently, increased CD8 T cells and a Th1 gene signature within the tumor microenvironment correlate with improved CRC patient outcomes (Galon et al., 2006). Yet our data suggest that increased homeostatic levels of CD8$^+$ IFNγ^+ T cells, associated with dysbiosis, can promote inflammation and tumorigenesis. To determine the activity of CD8 T cells within tumors of WT1 and WT2 mice, we analyzed the immune composition of tumor tissue ("tum") and non-tumor tissue adjacent to tumors ("adj") using flow cytometry. No differences in total T cells or CD4 T cells were measured between WT1 and WT2 mice in both tumor and adjacent tissues (Figures 7A and 7B). However, contrary to naive and acute inflammatory conditions, WT2 CD8 T cells are decreased in both tumor and adjacent tissue compared with WT1 tissues (Figure 7B). Furthermore, both intratumoral WT2 CD8 and CD4 T cells have reduced IFNγ responses compared with WT1 CD8 and CD4 T cells upon *ex vivo* stimulation (Figures 7C and 7D), whereas no differences in intratumoral CD4$^+$ IL-17$^+$ or CD4$^+$ Foxp3$^+$ cells were observed (Figures 7E and 7F).

On the basis of the pattern of increased CD8$^+$ IFNγ^+ T cells at baseline and during chronic inflammation followed by reduced CD8$^+$ IFNγ^+ T cells within the tumor microenvironment and adjacent normal tissue in WT2 mice, we hypothesized that the dysbiotic WT2 microbiome promotes T cell exhaustion. T cell exhaustion can occur as a result of prolonged antigen exposure and chronic inflammation (Wherry and Ahmed, 2004; Wherry et al., 2003) and is also observed with tumor-infiltrating lymphocytes, which can promote tumor progression (Baitsch et al., 2011; Fourcade et al., 2010; Grosso et al., 2009; Lee et al., 1999; Matsuzaki et al., 2010; Sakuishi et al., 2010). To determine if intratumoral WT2 T cells exhibit an exhausted phenotype, we measured inhibitory receptors typically expressed by exhausted T cells using flow cytometry. Indeed, there were greater numbers of PD-1$^+$ Lag-3$^+$ and PD-1$^+$ Tim-3$^+$ CD8 T cells within WT2 tumors compared with WT1 tumors (Figure 7G). Additionally, tumor-infiltrating WT2 CD4 T cells also exhibited increased PD-1 and Lag-3 expression compared with WT1 CD4 T cells (Figure 7H). Altogether, these data suggest that dysbiosis can lead to T cell exhaustion by chronically inducing IFNγ production in CD8 T cells, which may result in impaired immune surveillance and increased susceptibility to tumorigenesis.

DISCUSSION

In this study, we took advantage of a unique system in which two distinct microbial communities in WT B6 mice are associated with different disease outcomes to identify host-microbial interactions that underlie susceptibility to inflammation-associated tumorigenesis. WT2 mice, which develop significantly more tumors after AOM/DSS treatment than WT1 mice, have an altered microbiome that is associated with increased LP CD8$^+$ IFNγ^+ T cells at baseline and during acute inflammatory responses in the colon. Although CD8 T cells are known for their cytotoxic, anti-tumor activity, our results suggest that in the presence of dysbiosis, they can also have a pathogenic role by promoting damaging, chronic inflammation and consequently tumor development. Consistently, *Rag1*$^{-/-}$ and *Cd8*$^{-/-}$ mice transplanted with microbiomes from WT2 donor mice developed significantly fewer tumors. However, the absence of CD8 T cells in the presence of a WT2 microbiome does not completely suppress tumorigenesis, suggesting the possibility that WT2 microbiota can also promote tumorigenesis via CD8-independent mechanisms and/or CD8 T cells can also contribute to tumor suppression. Although there is significant evidence supporting a role of commensal-specific CD4 T cells in mediating inflammatory Th1 and Th17 responses (Cong et al., 1998; Sorini et al., 2018), less is known about the contribution of CD8 T cells in driving colon inflammation. CD8 T cells have been implicated in IBD, whereby increased colon LP activated cytotoxic CD8 T cells are associated with active disease (Müller et al., 1998). In certain mouse models, host antigen-reactive CD8 T cells have been shown to be major drivers of colitis (Nancey et al., 2006; Punit et al., 2015; Westendorf et al., 2006). However, whether WT2 microbiota promotes the generation of commensal-specific CD8 T cells to potentiate colitis-associated tumorigenesis remains to be determined.

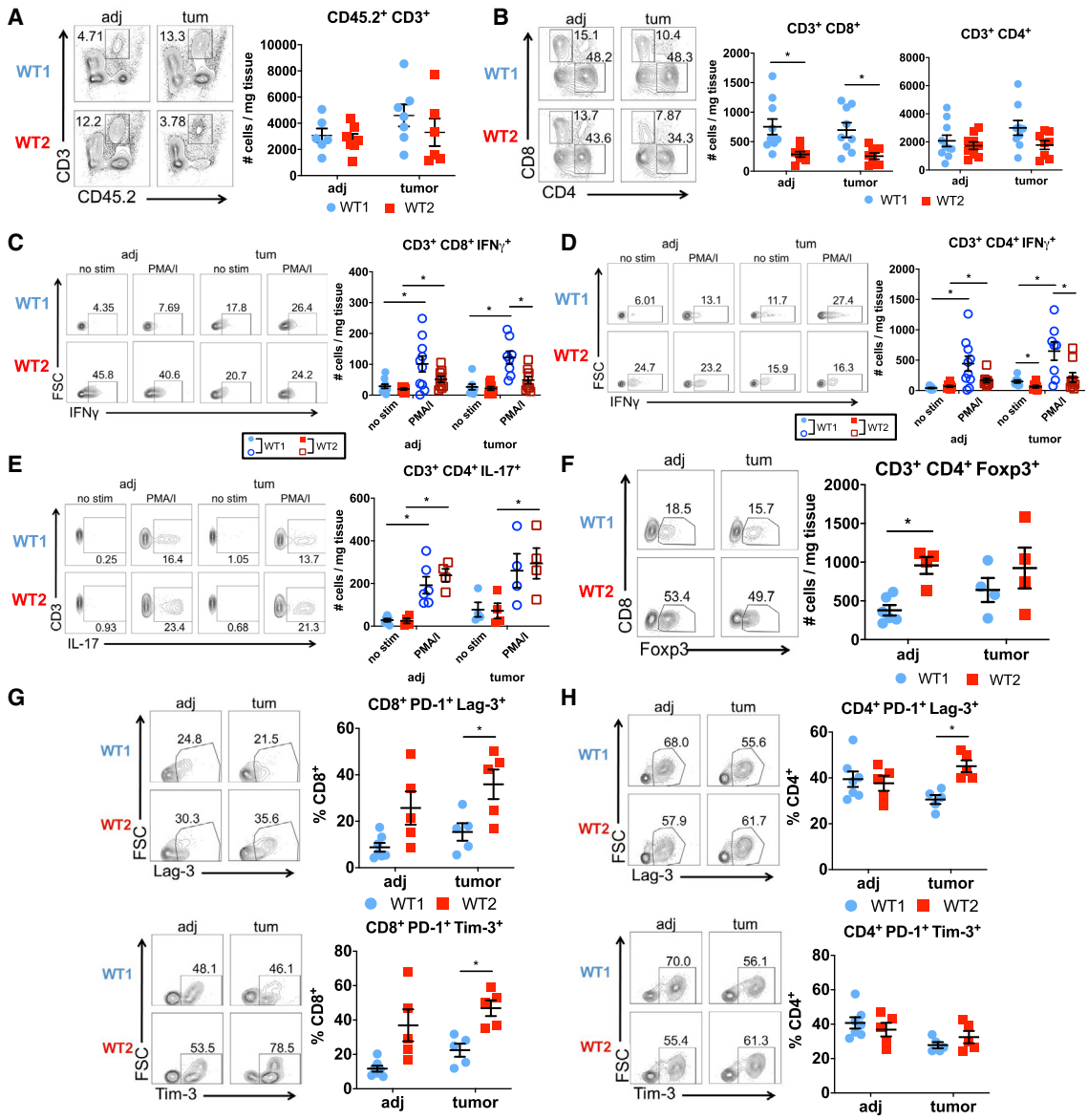

Figure 7. Intratumoral WT2 T Cells Display Decreased IFNγ Activity and Increased Exhaustion

(A and B) Numbers of T cells (A) and CD4 and CD8 T cells (B) in tumor ("tum") and adjacent ("adj") tissue from AOM/DSS-treated WT1 and WT2 mice as analyzed using flow cytometry on day 60. n = 6–10/group.

(C–F) Representative flow plots after *ex vivo* stimulation of cells for 4 h and analysis of IFNγ (N = 8–10/group), FoxP3, and IL-17 (n = 4–6/group).

(G and H) Representative flow plots and quantification of PD-1, Tim-3, and Lag-3 on CD8 (G) or CD4 T (H) cells. n = 5–7/group.

Data are mean ± SEM and are pooled from at least two independent experiments. *p < 0.05 by Mann-Whitney test.

How dysbiosis promotes the accumulation of activated $CD8^+$ $IFN\gamma^+$ T cells in naive WT2 mice is unclear and may be multifactorial in nature. It has been previously shown that *Bifidobacterium* is capable of priming DCs to enhance CD8 T cell proliferation and IFNγ production (Sivan et al., 2015). Similarly, we observed increased IL-12 production by BMDCs stimulated with HK WT2 microbiota. Therefore, it is possible that the presence of certain bacterial populations in the gut of WT2 mice selectively expands and primes the activation of colon LP CD8 T cells via DC activation. Gnotobiotic mouse studies also suggest that the accumulation of $CD8^+$ $IFN\gamma^+$ T cells is a result of chemokine induction by specific bacteria proximal to the intestinal epithelium (Tanoue et al., 2019); however, we did not observe any differences in epithelial production of CXCL9 or CXCL10 in WT1 and WT2 mice. Given that bacteria-produced metabolites can have immunomodulatory effects (Kim, 2018; Levy et al., 2016; Smith et al., 2013), it is also possible that WT2 microbiota-specific metabolites may contribute to increased colon LP $CD8^+$ $IFN\gamma^+$ T cells. For example, the gut microbiota can modulate levels of

all-trans-retinoic acid levels that can promote CD8 T cell responses in CRC (Bhattacharya et al., 2016).

Importantly, our results suggest a role of dysbiosis in promoting T cell exhaustion, which, within the tumor microenvironment, can reduce anti-tumor immunity. Specifically, in contrast to increased colon LP $CD8^+$ $IFN\gamma^+$ T cells in naive and acutely inflamed WT2 mice, there were significantly decreased tumor-infiltrating $CD8^+$ $IFN\gamma^+$ cells as well as in normal adjacent tissue. A potential explanation for the observed reduction in $CD8^+$ $IFN\gamma^+$ cells is that chronic stimulation and activation of intestinal LP CD8 T cells by WT2 gut microbiota lead to their exhaustion and result in reduced immune surveillance and ultimately increased tumor burden. Conversely, it is also possible that WT1 microbiota limits T cell exhaustion during the development of inflammation and tumors in the colon. Thus, it may be important to identify bacterial populations that not only induce protective $CD8^+$ $IFN\gamma^+$ responses within the tumor microenvironment but also attenuate T cell exhaustion to maximize anti-tumor immunity.

In this study, we identified several OTUs that were predictive of tumor susceptibility by analyzing the gut microbiomes of WT1 and WT2 mice as well as of mice from multiple fecal transfer experiments with hybrid microbiomes. We and others have used similar approaches and statistical tools to identify differential OTUs between groups that correlate with disease outcomes (Caruso et al., 2019; Seregin et al., 2017; Surana and Kasper, 2017; Zackular et al., 2015). Here, the low or high tumor burdens of AOM/DSS-treated mice cannot be attributed to just a single bacteria species or family. For example, the bacteria family *Prevotellaceae* is increased in naive WT2 mice and strongly predictive of high tumor burdens, while *Lachnospiraceae* is significantly associated with decreased inflammation-associated tumorigenesis. Decreased *Lachnospiraceae* have been found in IBD and CRC patients (Morgan et al., 2012; Wang et al., 2012), suggesting that they have anti-inflammatory function, possibly via butyrate production (Wang et al., 2012). In contrast, *Prevotellaceae* are enriched in IBD and CRC patients and are also associated with increased susceptibility to DSS-induced colitis in mice, which suggests that they may be pro-inflammatory (Elinav et al., 2011; Flemer et al., 2017; Sobhani et al., 2011; Wang et al., 2012). Similarly, a member of the *Ruminococcaceae* was associated with high tumor burdens, and *Ruminococcaceae* have also been found to be enriched in IBD and CRC patients (Joossens et al., 2011; Wang et al., 2012). Furthermore, a phylogenetic tree based on 16S rRNA sequence similarity suggests that the OTU candidates associated with different tumor burdens but from the same family are evolutionarily distinct from one another (Figure 4C) (Clarridge, 2004; Woese, 1987). Regardless, as we have only identified a correlation between the identified OTUs and tumor outcomes, it still remains to be determined whether these bacteria regulate CD8 T cell responses and tumor susceptibility alone or via interactions with other bacterial populations.

There has been significant interest in optimizing microbiome transfer to control for or determine microbiome-specific effects on phenotype. The gold standard is fecal transplantation of donor microbiota into recipient GF mice. In this study, the transfer of WT1 or WT2 microbiomes and their corresponding tumor phenotype was optimal using this system. Cohousing is a widely used method of microbiome transfer between mice of dissimilar microbiome compositions in host-microbiome association studies, but the optimal length of time of cohousing and ratio of mice harboring two different communities in a cage remain unclear. Here, we show that 4 weeks of 2:2 cohousing resulted in poor microbiome and phenotype transfer. Transfer was significantly improved with 6 weeks of 1:1 cohousing; however, microbiome analyses demonstrated that the transfer was still incomplete, with significant differences in OTU membership between cohoused mice by LEfSe (data not shown), likely explaining the intermediate tumor phenotype. Generation of hybrid microbiomes and incomplete transfer by cohousing were also observed by others (Caruso et al., 2019; Robertson et al., 2019; Surana and Kasper, 2017). In this study, cross-fostering provided better microbiome transfer from WT1 and WT2 mothers to WT2 and WT1 pups, respectively, than cohousing, demonstrating the strong influence of maternal transmission of the microbiome to offspring, although as with 1:1 cohousing, significant differences in microbiome composition remained. Despite the improvement in microbiome transfer, the tumor phenotype of cross-fostered mice remained intermediate between control WT1 and WT2 mice. It is possible that the transfer of WT1 and WT2 microbiomes was incomplete with these methods given the difficulty of transferring mucosa-associated adherent bacteria (Robertson et al., 2019). Alternatively, the lack of complete phenotype transmissibility with either cohousing or cross-fostering may also reflect the poor survivability of obligate anaerobes outside the colon. Interestingly, on the basis of thetaYC dissimilarity, we observed effective microbiome transfer in mice that were gavaged with cecal and fecal contents from donor mice after antibiotic depletion, although not necessarily as complete as in GF mice. Nonetheless, this approach may still be a reasonable alternative to GF mice in determining the effects of specific microbial communities on phenotype. Other groups also observed similar transfer results by this method (Le Roy et al., 2018; Shen et al., 2015; Staley et al., 2017). Nevertheless, further studies are needed to determine the antibiotic combination, length of treatment, and number of gavages for optimal transfer of microbiota and phenotype.

In summary, our data demonstrate a role of the gut microbiome in altering CD8 T cell activity in the colon LP to affect tumorigenesis through early CD8 T cell activation, which can have long-term negative consequences by increasing susceptibility to inflammation and exhaustion, which can result in colon tumorigenesis. Future studies are needed to determine the mechanism by which the microbiota activates CD8 T cells and promotes their exhaustion.

STAR★METHODS

Detailed methods are provided in the online version of this paper and include the following:

- KEY RESOURCES TABLE
- LEAD CONTACT AND MATERIALS AVAILABILITY
- EXPERIMENTAL MODEL AND SUBJECT DETAILS
  - Animals

SUPPLEMENTAL INFORMATION

Supplemental Information can be found online at https://doi.org/10.1016/j.celrep.2020.03.035.

ACKNOWLEDGMENTS

We thank Joseph Zackular, Nielsen Baxter, Nicholas Pudlo, Gabriel Nuñez, Asma Nusrat, Yatrik Shah, and Sergey Seregin for their advice and critical manuscript reading, and the University of Michigan (UM) Flow Cytometry, Germ-Free and Gnotobiotic, Cancer Center Immunology, DNA Sequencing, Histology, and Microscopy Cores for technical support. This work was supported by a UM Rackham Research Grant and NIH grant T32 AI007413 (A.I.Y.) and NIH grant R01 CA166879, an American Cancer Society Research Scholar Grant, and the Tom Liu Memorial Golf Tournament Fund from the UM Rogel Cancer Center (G.Y.C.).

AUTHOR CONTRIBUTIONS

Conceptualization and Methodology, A.I.Y. and G.Y.C.; Formal Analysis, A.I.Y., L.Z., and G.Y.C.; Investigation, A.I.Y., L.Z., K.A.E., S.H., J.C., S.P., J.B., A.G., D.M., M.H., J.M.-C., J.W., C.K., E.C.M., and G.Y.C.; Histologic Interpretation and Scoring, K.A.E.; Writing – Original Draft, A.I.Y. and G.Y.C.; Writing – Review & Editing, A.I.Y., L.Z., and G.Y.C.; Funding Acquisition, A.I.Y. and G.Y.C.; Resources, P.D.S. and E.C.M.

DECLARATION OF INTERESTS

The authors declare no competing interests.

Received: August 19, 2019
Revised: February 13, 2020
Accepted: March 12, 2020
Published: April 7, 2020

REFERENCES

Abt, M.C., Osborne, L.C., Monticelli, L.A., Doering, T.A., Alenghat, T., Sonnenberg, G.F., Paley, M.A., Antenus, M., Williams, K.L., Erikson, J., et al. (2012). Commensal bacteria calibrate the activation threshold of innate antiviral immunity. Immunity *37*, 158–170.

Ahn, J., Sinha, R., Pei, Z., Dominianni, C., Wu, J., Shi, J., Goedert, J.J., Hayes, R.B., and Yang, L. (2013). Human gut microbiome and risk for colorectal cancer. J. Natl. Cancer Inst. *105*, 1907–1911.

Arnold, M., Sierra, M.S., Laversanne, M., Soerjomataram, I., Jemal, A., and Bray, F. (2017). Global patterns and trends in colorectal cancer incidence and mortality. Gut *66*, 683–691.

Arthur, J.C., Perez-Chanona, E., Mühlbauer, M., Tomkovich, S., Uronis, J.M., Fan, T.J., Campbell, B.J., Abujamel, T., Dogan, B., Rogers, A.B., et al. (2012). Intestinal inflammation targets cancer-inducing activity of the microbiota. Science *338*, 120–123.

Atarashi, K., Tanoue, T., Shima, T., Imaoka, A., Kuwahara, T., Momose, Y., Cheng, G., Yamasaki, S., Saito, T., Ohba, Y., et al. (2011). Induction of colonic regulatory T cells by indigenous Clostridium species. Science *331*, 337–341.

Baitsch, L., Baumgaertner, P., Devêvre, E., Raghav, S.K., Legat, A., Barba, L., Wieckowski, S., Bouzourene, H., Deplancke, B., Romero, P., et al. (2011). Exhaustion of tumor-specific $CD8^+$ T cells in metastases from melanoma patients. J. Clin. Invest. *121*, 2350–2360.

Baxter, N.T., Zackular, J.P., Chen, G.Y., and Schloss, P.D. (2014). Structure of the gut microbiome following colonization with human feces determines colonic tumor burden. Microbiome *2*, 20.

Becker, C., Fantini, M.C., Schramm, C., Lehr, H.A., Wirtz, S., Nikolaev, A., Burg, J., Strand, S., Kiesslich, R., Huber, S., et al. (2004). TGF-beta suppresses tumor progression in colon cancer by inhibition of IL-6 trans-signaling. Immunity *21*, 491–501.

Belkaid, Y., and Hand, T.W. (2014). Role of the microbiota in immunity and inflammation. Cell *157*, 121–141.

Ben-Sasson, S.Z., Wang, K., Cohen, J., and Paul, W.E. (2013). IL-1β strikingly enhances antigen-driven CD4 and CD8 T-cell responses. Cold Spring Harb. Symp. Quant. Biol. *78*, 117–124.

Benjamini, Y., and Yekutieli, D. (2001). The control of the false discovery rate in multiple testing under dependency. Ann. Stat. *29*, 1165–1188.

Bhattacharya, N., Yuan, R., Prestwood, T.R., Penny, H.L., DiMaio, M.A., Reticker-Flynn, N.E., Krois, C.R., Kenkel, J.A., Pham, T.D., Carmi, Y., et al. (2016). Normalizing microbiota-induced retinoic acid deficiency stimulates protective CD8(+) T cell-mediated immunity in colorectal cancer. Immunity *45*, 641–655.

Breiman, L. (2001). Random forests. Mach. Learn. *45*, 5–32.

Brzoza, K.L., Rockel, A.B., and Hiltbold, E.M. (2004). Cytoplasmic entry of Listeria monocytogenes enhances dendritic cell maturation and T cell differentiation and function. J. Immunol. *173*, 2641–2651.

Caruso, R., Ono, M., Bunker, M.E., Nunez, G., and Inohara, N. (2019). Dynamic and asymmetric changes of the microbial communities after cohousing in laboratory mice. Cell Rep. *27*, 3401–3412.e3.

Castro, F., Cardoso, A.P., Gonçalves, R.M., Serre, K., and Oliveira, M.J. (2018). Interferon-gamma at the crossroads of tumor immune surveillance or evasion. Front. Immunol. *9*, 847.

Chassaing, B., Srinivasan, G., Delgado, M.A., Young, A.N., Gewirtz, A.T., and Vijay-Kumar, M. (2012). Fecal lipocalin 2, a sensitive and broadly dynamic non-invasive biomarker for intestinal inflammation. PLoS ONE *7*, e44328.

Chassaing, B., Aitken, J.D., Malleshappa, M., and Vijay-Kumar, M. (2014). Dextran sulfate sodium (DSS)-induced colitis in mice. Curr. Protoc. Immunol. *104*, 15.25.1–15.25.14.

Chen, G.Y., Shaw, M.H., Redondo, G., and Núñez, G. (2008). The innate immune receptor Nod1 protects the intestine from inflammation-induced tumorigenesis. Cancer Res. *68*, 10060–10067.

Clarridge, J.E., 3rd. (2004). Impact of 16S rRNA gene sequence analysis for identification of bacteria on clinical microbiology and infectious diseases. Clin. Microbiol. Rev. *17*, 840–862.

Cong, Y., Brandwein, S.L., McCabe, R.P., Lazenby, A., Birkenmeier, E.H., Sundberg, J.P., and Elson, C.O. (1998). CD4+ T cells reactive to enteric bacterial antigens in spontaneously colitic C3H/HeJBir mice: increased T helper cell type 1 response and ability to transfer disease. J. Exp. Med. *187*, 855–864.

Curtsinger, J.M., Schmidt, C.S., Mondino, A., Lins, D.C., Kedl, R.M., Jenkins, M.K., and Mescher, M.F. (1999). Inflammatory cytokines provide a third signal for activation of naive CD4+ and CD8+ T cells. J. Immunol. *162*, 3256–3262.

Daft, J.G., Ptacek, T., Kumar, R., Morrow, C., and Lorenz, R.G. (2015). Cross-fostering immediately after birth induces a permanent microbiota shift that is shaped by the nursing mother. Microbiome *3*, 17.

De Robertis, M., Massi, E., Poeta, M.L., Carotti, S., Morini, S., Cecchetelli, L., Signori, E., and Fazio, V.M. (2011). The AOM/DSS murine model for the study of colon carcinogenesis: From pathways to diagnosis and therapy studies. J. Carcinog. *10*, 9.

Eaden, J.A., Abrams, K.R., and Mayberry, J.F. (2001). The risk of colorectal cancer in ulcerative colitis: a meta-analysis. Gut *48*, 526–535.

Edgar, R. (2018). Taxonomy annotation and guide tree errors in 16S rRNA databases. PeerJ *6*, e5030.

Elinav, E., Strowig, T., Kau, A.L., Henao-Mejia, J., Thaiss, C.A., Booth, C.J., Peaper, D.R., Bertin, J., Eisenbarth, S.C., Gordon, J.I., and Flavell, R.A. (2011). NLRP6 inflammasome regulates colonic microbial ecology and risk for colitis. Cell *145*, 745–757.

Excoffier, L., Smouse, P.E., and Quattro, J.M. (1992). Analysis of molecular variance inferred from metric distances among DNA haplotypes: application to human mitochondrial DNA restriction data. Genetics *131*, 479–491.

Flemer, B., Lynch, D.B., Brown, J.M.R., Jeffery, I.B., Ryan, F.J., Claesson, M.J., O'Riordain, M., Shanahan, F., and O'Toole, P.W. (2017). Tumour-associated and non-tumour-associated microbiota in colorectal cancer. Gut *66*, 633–643.

Fourcade, J., Sun, Z., Benallaoua, M., Guillaume, P., Luescher, I.F., Sander, C., Kirkwood, J.M., Kuchroo, V., and Zarour, H.M. (2010). Upregulation of Tim-3 and PD-1 expression is associated with tumor antigen-specific CD8+ T cell dysfunction in melanoma patients. J. Exp. Med. *207*, 2175–2186.

Furusawa, Y., Obata, Y., Fukuda, S., Endo, T.A., Nakato, G., Takahashi, D., Nakanishi, Y., Uetake, C., Kato, K., Kato, T., et al. (2013). Commensal microbe-derived butyrate induces the differentiation of colonic regulatory T cells. Nature *504*, 446–450.

Galon, J., Costes, A., Sanchez-Cabo, F., Kirilovsky, A., Mlecnik, B., Lagorce-Pagès, C., Tosolini, M., Camus, M., Berger, A., Wind, P., et al. (2006). Type, density, and location of immune cells within human colorectal tumors predict clinical outcome. Science *313*, 1960–1964.

Geva-Zatorsky, N., Sefik, E., Kua, L., Pasman, L., Tan, T.G., Ortiz-Lopez, A., Yanortsang, T.B., Yang, L., Jupp, R., Mathis, D., et al. (2017). Mining the human gut microbiota for immunomodulatory organisms. Cell *168*, 928–943.e11.

Greten, F.R., Eckmann, L., Greten, T.F., Park, J.M., Li, Z.W., Egan, L.J., Kagnoff, M.F., and Karin, M. (2004). IKKbeta links inflammation and tumorigenesis in a mouse model of colitis-associated cancer. Cell *118*, 285–296.

Grosso, J.F., Goldberg, M.V., Getnet, D., Bruno, T.C., Yen, H.-R., Pyle, K.J., Hipkiss, E., Vignali, D.A.A., Pardoll, D.M., and Drake, C.G. (2009). Functionally distinct LAG-3 and PD-1 subsets on activated and chronically stimulated CD8 T cells. J. Immunol. *182*, 6659–6669.

Gur, C., Ibrahim, Y., Isaacson, B., Yamin, R., Abed, J., Gamliel, M., Enk, J., Bar-On, Y., Stanietsky-Kaynan, N., Coppenhagen-Glazer, S., et al. (2015). Binding of the Fap2 protein of Fusobacterium nucleatum to human inhibitory receptor TIGIT protects tumors from immune cell attack. Immunity *42*, 344–355.

Hehemann, J.H., Kelly, A.G., Pudlo, N.A., Martens, E.C., and Boraston, A.B. (2012). Bacteria of the human gut microbiome catabolize red seaweed glycans with carbohydrate-active enzyme updates from extrinsic microbes. Proc. Natl. Acad. Sci. U S A *109*, 19786–19791.

Joossens, M., Huys, G., Cnockaert, M., Preter, V.D., Verbeke, K., Rutgeerts, P., Vandamme, P., and Vermeire, S. (2011). Dysbiosis of the faecal microbiota in patients with Crohn's disease and their unaffected relatives. Gut *60*, 631–637.

Kennedy, E.A., King, K.Y., and Baldridge, M.T. (2018). Mouse microbiota models: comparing germ-free mice and antibiotics treatment as tools for modifying gut bacteria. Front. Physiol. *9*, 1534.

Kim, C.H. (2018). Immune regulation by microbiome metabolites. Immunology *154*, 220–229.

Kozich, J.J., Westcott, S.L., Baxter, N.T., Highlander, S.K., and Schloss, P.D. (2013). Development of a dual-index sequencing strategy and curation pipeline for analyzing amplicon sequence data on the MiSeq Illumina sequencing platform. Appl. Environ. Microbiol. *79*, 5112–5120.

Le Roy, T., Debédat, J., Marquet, F., Da-Cunha, C., Ichou, F., Guerre-Millo, M., Kapel, N., Aron-Wisnewsky, J., and Clément, K. (2018). Comparative evaluation of microbiota engraftment following fecal microbiota transfer in mice models: age, kinetic and microbial status matter. Front. Microbiol. *9*, 3289.

Lee, P.P., Yee, C., Savage, P.A., Fong, L., Brockstedt, D., Weber, J.S., Johnson, D., Swetter, S., Thompson, J., Greenberg, P.D., et al. (1999). Characterization of circulating T cells specific for tumor-associated antigens in melanoma patients. Nat. Med. *5*, 677–685.

Levy, M., Thaiss, C.A., and Elinav, E. (2016). Metabolites: messengers between the microbiota and the immune system. Genes Dev. *30*, 1589–1597.

Madeira, F., Park, Y.M., Lee, J., Buso, N., Gur, T., Madhusoodanan, N., Basutkar, P., Tivey, A.R.N., Potter, S.C., Finn, R.D., et al. (2019). The EMBL-EBI search and sequence analysis tools APIs in 2019. Nucleic Acids Res. *47*, W636–W641.

Mager, L.F., Wasmer, M.H., Rau, T.T., and Krebs, P. (2016). Cytokine-induced modulation of colorectal cancer. Front. Oncol. *6*, 96.

Markman, J.L., and Shiao, S.L. (2015). Impact of the immune system and immunotherapy in colorectal cancer. J. Gastrointest. Oncol. *6*, 208–223.

Maslowski, K.M., Vieira, A.T., Ng, A., Kranich, J., Sierro, F., Yu, D., Schilter, H.C., Rolph, M.S., Mackay, F., Artis, D., et al. (2009). Regulation of inflammatory responses by gut microbiota and chemoattractant receptor GPR43. Nature *461*, 1282–1286.

Matsuzaki, J., Gnjatic, S., Mhawech-Fauceglia, P., Beck, A., Miller, A., Tsuji, T., Eppolito, C., Qian, F., Lele, S., Shrikant, P., et al. (2010). Tumor-infiltrating NY-ESO-1-specific CD8+ T cells are negatively regulated by LAG-3 and PD-1 in human ovarian cancer. Proc. Natl. Acad. Sci. U S A *107*, 7875–7880.

Moore, R.J., and Stanley, D. (2016). Experimental design considerations in microbiota/inflammation studies. Clin .Transl. Immunol. *5*, e92.

Morgan, X.C., Tickle, T.L., Sokol, H., Gevers, D., Devaney, K.L., Ward, D.V., Reyes, J.A., Shah, S.A., LeLeiko, N., Snapper, S.B., et al. (2012). Dysfunction of the intestinal microbiome in inflammatory bowel disease and treatment. Genome Biol. *13*, R79.

Müller, S., Lory, J., Corazza, N., Griffiths, G.M., Z'graggen, K., Mazzucchelli, L., Kappeler, A., and Mueller, C. (1998). Activated CD4+ and CD8+ cytotoxic cells are present in increased numbers in the intestinal mucosa from patients with active inflammatory bowel disease. Am. J. Pathol. *152*, 261–268.

Műzes, G., Molnár, B., and Sipos, F. (2012). Regulatory T cells in inflammatory bowel diseases and colorectal cancer. World J. Gastroenterol. *18*, 5688–5694.

Nancey, S., Holvöet, S., Graber, I., Joubert, G., Philippe, D., Martin, S., Nicolas, J.F., Desreumaux, P., Flourié, B., and Kaiserlian, D. (2006). CD8+ cytotoxic T cells induce relapsing colitis in normal mice. Gastroenterology *131*, 485–496.

Neufert, C., Becker, C., and Neurath, M.F. (2007). An inducible mouse model of colon carcinogenesis for the analysis of sporadic and inflammation-driven tumor progression. Nat. Protoc. *2*, 1998–2004.

Nougayrède, J.P., Homburg, S., Taieb, F., Boury, M., Brzuszkiewicz, E., Gottschalk, G., Buchrieser, C., Hacker, J., Dobrindt, U., and Oswald, E. (2006). Escherichia coli induces DNA double-strand breaks in eukaryotic cells. Science *313*, 848–851.

Pagès, F., Berger, A., Camus, M., Sanchez-Cabo, F., Costes, A., Molidor, R., Mlecnik, B., Kirilovsky, A., Nilsson, M., Damotte, D., et al. (2005). Effector memory T cells, early metastasis, and survival in colorectal cancer. N. Engl. J. Med. *353*, 2654–2666.

Pernot, S., Terme, M., Voron, T., Colussi, O., Marcheteau, E., Tartour, E., and Taieb, J. (2014). Colorectal cancer and immunity: what we know and perspectives. World J. Gastroenterol. *20*, 3738–3750.

Pruesse, E., Quast, C., Knittel, K., Fuchs, B.M., Ludwig, W., Peplies, J., and Glöckner, F.O. (2007). SILVA: a comprehensive online resource for quality checked and aligned ribosomal RNA sequence data compatible with ARB. Nucleic Acids Res. *35*, 7188–7196.

Punit, S., Dube, P.E., Liu, C.Y., Girish, N., Washington, M.K., and Polk, D.B. (2015). Tumor necrosis factor receptor 2 restricts the pathogenicity of CD8(+) T cells in mice with colitis. Gastroenterology *149*, 993–1005.e2.

Razi, S., Baradaran Noveiry, B., Keshavarz-Fathi, M., and Rezaei, N. (2019). IL-17 and colorectal cancer: From carcinogenesis to treatment. Cytokine *116*, 7–12.

Robertson, S.J., Lemire, P., Maughan, H., Goethel, A., Turpin, W., Bedrani, L., Guttman, D.S., Croitoru, K., Girardin, S.E., and Philpott, D.J. (2019). Comparison of co-housing and littermate methods for microbiota standardization in mouse models. Cell Rep. *27*, 1910–1919.e2.

Sakuishi, K., Apetoh, L., Sullivan, J.M., Blazar, B.R., Kuchroo, V.K., and Anderson, A.C. (2010). Targeting Tim-3 and PD-1 pathways to reverse T cell exhaustion and restore anti-tumor immunity. J. Exp. Med. *207*, 2187–2194.

Schloss, P.D., Westcott, S.L., Ryabin, T., Hall, J.R., Hartmann, M., Hollister, E.B., Lesniewski, R.A., Oakley, B.B., Parks, D.H., Robinson, C.J., et al. (2009). Introducing mothur: open-source, platform-independent, community-supported software for describing and comparing microbial communities. Appl. Environ. Microbiol. *75*, 7537–7541.

Segata, N., Izard, J., Waldron, L., Gevers, D., Miropolsky, L., Garrett, W.S., and Huttenhower, C. (2011). Metagenomic biomarker discovery and explanation. Genome Biol. *12*, R60.

Seregin, S.S., Golovchenko, N., Schaf, B., Chen, J., Pudlo, N.A., Mitchell, J., Baxter, N.T., Zhao, L., Schloss, P.D., Martens, E.C., et al. (2017). NLRP6 protects IL10−/− mice from colitis by limiting colonization of Akkermansia muciniphila. Cell Rep. *19*, 733–745.

Shen, T.C., Albenberg, L., Bittinger, K., Chehoud, C., Chen, Y.Y., Judge, C.A., Chau, L., Ni, J., Sheng, M., Lin, A., et al. (2015). Engineering the gut microbiota to treat hyperammonemia. J. Clin. Invest. *125*, 2841–2850.

Sivan, A., Corrales, L., Hubert, N., Williams, J.B., Aquino-Michaels, K., Earley, Z.M., Benyamin, F.W., Lei, Y.M., Jabri, B., Alegre, M.L., et al. (2015). Commensal Bifidobacterium promotes antitumor immunity and facilitates anti-PD-L1 efficacy. Science *350*, 1084–1089.

Smith, P.M., Howitt, M.R., Panikov, N., Michaud, M., Gallini, C.A., Bohlooly-Y, M., Glickman, J.N., and Garrett, W.S. (2013). The microbial metabolites, short-chain fatty acids, regulate colonic Treg cell homeostasis. Science *341*, 569–573.

Sobhani, I., Tap, J., Roudot-Thoraval, F., Roperch, J.P., Letulle, S., Langella, P., Corthier, G., Tran Van Nhieu, J., and Furet, J.P. (2011). Microbial dysbiosis in colorectal cancer (CRC) patients. PLoS ONE *6*, e16393.

Sorini, C., Cardoso, R.F., Gagliani, N., and Villablanca, E.J. (2018). Commensal bacteria-specific $CD4^+$ T cell responses in health and disease. Front. Immunol. *9*, 2667.

Staley, C., Kaiser, T., Beura, L.K., Hamilton, M.J., Weingarden, A.R., Bobr, A., Kang, J., Masopust, D., Sadowsky, M.J., and Khoruts, A. (2017). Stable engraftment of human microbiota into mice with a single oral gavage following antibiotic conditioning. Microbiome *5*, 87.

Surana, N.K., and Kasper, D.L. (2017). Moving beyond microbiome-wide associations to causal microbe identification. Nature *552*, 244–247.

Suzuki, R., Kohno, H., Sugie, S., and Tanaka, T. (2004). Sequential observations on the occurrence of preneoplastic and neoplastic lesions in mouse colon treated with azoxymethane and dextran sodium sulfate. Cancer Sci. *95*, 721–727.

Tanaka, T., Kohno, H., Suzuki, R., Yamada, Y., Sugie, S., and Mori, H. (2003). A novel inflammation-related mouse colon carcinogenesis model induced by azoxymethane and dextran sodium sulfate. Cancer Sci. *94*, 965–973.

Tanoue, T., Morita, S., Plichta, D.R., Skelly, A.N., Suda, W., Sugiura, Y., Narushima, S., Vlamakis, H., Motoo, I., Sugita, K., et al. (2019). A defined commensal consortium elicits CD8 T cells and anti-cancer immunity. Nature *565*, 600–605.

Toubai, T., Fujiwara, H., Rossi, C., Riwes, M., Tamaki, H., Zajac, C., Liu, C., Mathew, A.V., Byun, J., Oravecz-Wilson, K., et al. (2019). Host NLRP6 exacerbates graft-versus-host disease independent of gut microbial composition. Nat. Microbiol. *4*, 800–812.

Trinchieri, G. (1998). Interleukin-12: a cytokine at the interface of inflammation and immunity. Adv. Immunol. *70*, 83–243.

Wang, T., Cai, G., Qiu, Y., Fei, N., Zhang, M., Pang, X., Jia, W., Cai, S., and Zhao, L. (2012). Structural segregation of gut microbiota between colorectal cancer patients and healthy volunteers. ISME J. *6*, 320–329.

Westendorf, A.M., Fleissner, D., Deppenmeier, S., Gruber, A.D., Bruder, D., Hansen, W., Liblau, R., and Buer, J. (2006). Autoimmune-mediated intestinal inflammation-impact and regulation of antigen-specific CD8+ T cells. Gastroenterology *131*, 510–524.

Wherry, E.J., and Ahmed, R. (2004). Memory CD8 T-cell differentiation during viral infection. J. Virol. *78*, 5535–5545.

Wherry, E.J., Blattman, J.N., Murali-Krishna, K., van der Most, R., and Ahmed, R. (2003). Viral persistence alters CD8 T-cell immunodominance and tissue distribution and results in distinct stages of functional impairment. J. Virol. *77*, 4911–4927.

White, J.R., Nagarajan, N., and Pop, M. (2009). Statistical methods for detecting differentially abundant features in clinical metagenomic samples. PLoS Comput. Biol. *5*, e1000352.

Woese, C.R. (1987). Bacterial evolution. Microbiol. Rev. *51*, 221–271.

Wu, S., Rhee, K.J., Albesiano, E., Rabizadeh, S., Wu, X., Yen, H.R., Huso, D.L., Brancati, F.L., Wick, E., McAllister, F., et al. (2009). A human colonic commensal promotes colon tumorigenesis via activation of T helper type 17 T cell responses. Nat. Med. *15*, 1016–1022.

Zackular, J.P., Baxter, N.T., Iverson, K.D., Sadler, W.D., Petrosino, J.F., Chen, G.Y., and Schloss, P.D. (2013). The gut microbiome modulates colon tumorigenesis. MBio *4*, e00692-13.

Zackular, J.P., Rogers, M.A., Ruffin, M.T., 4th, and Schloss, P.D. (2014). The human gut microbiome as a screening tool for colorectal cancer. Cancer Prev. Res. (Phila.) *7*, 1112–1121.

Zackular, J.P., Baxter, N.T., Chen, G.Y., and Schloss, P.D. (2015). Manipulation of the gut microbiota reveals role in colon tumorigenesis. MSphere *1*, 1.

Ze, X., Duncan, S.H., Louis, P., and Flint, H.J. (2012). Ruminococcus bromii is a keystone species for the degradation of resistant starch in the human colon. ISME J. *6*, 1535–1543.

Zhan, Y., Chen, P.J., Sadler, W.D., Wang, F., Poe, S., Núñez, G., Eaton, K.A., and Chen, G.Y. (2013). Gut microbiota protects against gastrointestinal tumorigenesis caused by epithelial injury. Cancer Res. *73*, 7199–7210.

Zhan, Y., Seregin, S.S., Chen, J., and Chen, G.Y. (2016). Nod1 limits colitis-associated tumorigenesis by regulating IFN-γ production. J. Immunol. *196*, 5121–5129.

STAR★METHODS

KEY RESOURCES TABLE

REAGENT or RESOURCE	SOURCE	IDENTIFIER
Antibodies		
CD3 APC-Cy7 clone 145-2C11	BioLegend	Cat#100330; AB_1877170
CD3 PE-Cy7 clone 17A2	BioLegend	Cat#100220; AB_1732057
CD3 FITC clone 145-2C11	BioLegend	Cat#100204; AB_312661
CD45.2 BV421 clone 104	BioLegend	Cat#109832; AB_2565511
CD4 APC clone GK1.5	eBioscience	Cat#17-004-82; AB_469320
CD8 PerCP-Cy5.5 clone 53-6.7	BioLegend	Cat#100732; AB_893423
CD8 APC-Cy7 clone 53-6.7	BioLegend	Cat#100714; AB_312753
CD69 APC clone H1.2F3	BioLegend	Cat#104514; AB_492843
CD44 PE clone IM7	BioLegend	Cat#103007; AB_312958
CD62L APC-Cy7 clone MEL-14	BioLegend	Cat#104427; AB_830798
Tim-3 PerCP-Cy5.5 clone B8.2C12	BioLegend	Cat#134011; AB_2632735
PD-1 PE-Cy7 clone RMP1-30	BioLegend	Cat#109109; AB_572016
Lag-3 PE clone C9B7W	BioLegend	Cat#125207; AB_2133344
IFNγ PE-Cy7 clone XMG1.2	BioLegend	Cat#505826; AB_2295770
IL-17 FITC clone TC11-18H10.1	BioLegend	Cat#506907; AB_536009
Foxp3 PE clone FJK-16 s	eBioscience	Cat#12-5773-80; AB_465936
NK1.1 PerCP-Cy5.5 clone PK136	BD PharMingen	Cat#561111
Ly6C FITC clone HK1.4	BioLegend	Cat#128005; AB_1186134
Ly6G PE-Cy7 clone 1A8	BioLegend	Cat#127617; AB_1877262
CD11b PE clone M1/70	BD PharMingen	Cat#561689; AB_394775
CD11c APC clone N418	BioLegend	Cat#117310; AB_313779
B220 Pacific Blue clone RA3-6B2	BioLegend	Cat#103227; AB_492876
CD103 PE clone 2E7	BioLegend	Cat#121405; AB_535948
Chemicals, Peptides, and Recombinant Proteins		
Azoxymethane (AOM)	Sigma Aldrich	Cat#A5486
Dithiothreitol (DTT)	Invitrogen	Cat#ILT15508013
AccuGENe 0.5 M EDTA Solution	Lonza	Cat#BMA51201
Deoxyribonuclease I	Worthington	Cat#LS002007
Collagenase, Type 3	Worthington	Cat#LS004183
Recombinant Murine GM-CSF	Peprotech	Cat#315-03
Percoll	GE Healthcare Life Sciences	Cat#17089101
Phorbol 12-myristate 13-acetate	Sigma Aldrich	Cat#P8139-5MG
Ionomycin	Sigma Aldrich	Cat#I9657
BD GolgiStop Protein Transport Inhibitor	BD	Cat#554724
Fluconazole	Sigma Aldrich	Cat#PHR1160
Vancomycin Hydrochloride, USP	Pfizer	N/A
Streptomycin sulfate salt	Sigma Aldrich	Cat#S6501
Metronidazole	Sigma Aldrich	Cat#M1547
BHI	BD	Cat#237500
Defibrinated Horse Blood	Quad Five	Cat#210
Granulated Agar	Thermo Fisher Scientific	Cat#BP9744-500
Bacto Agar	BD	Cat#DF0140-01-0
Beef extract	Sigma-Aldrich	Cat#B4888

(*Continued on next page*)

Continued

REAGENT or RESOURCE	SOURCE	IDENTIFIER
Pancreatic digest of casein	BioWorld	Cat#30620060-1
Yeast extract	Fluka Analytical	Cat#70161
Dipotassium phosphate	Thermo Fisher Scientific	Cat#BP363-500
Cysteine	Sigma-Aldrich	Cat#C7352
Glucose	Sigma-Aldrich	Cat#158968
Galactose	Sigma-Aldrich	Cat#G0625
Fructose	Sigma-Aldrich	Cat#F0127
Mannose	Acros Organics	Cat#150600
N-acetyl glucosamine	Sigma-Aldrich	Cat#A3286
Xylose	Sigma-Aldrich	Cat#X3877
Hematin	Sigma-Aldrich	Cat#H3281
Histidine	Sigma-Aldrich	Cat#H8000
Menadione	Sigma-Aldrich	Cat#M5625
Cyanocobalamin	Sigma-Aldrich	Cat#V2876
p-Aminobenzoic acid	Sigma-Aldrich	Cat#A9878
Folic acid	Sigma-Aldrich	Cat#F7876
Biotin	Sigma-Aldrich	Cat#B4501
Nicotinic acid	Sigma-Aldrich	Cat#N4126
Calcium pantothenate	Sigma-Aldrich	Cat#P2250
Riboflavin	Sigma-Aldrich	Cat#R7649
Thiamine HCl	Sigma-Aldrich	Cat#T4625
Pyridoxine HCl	Sigma-Aldrich	Cat#P9755
Thioctic acid	Sigma-Aldrich	Cat#T5625
Adenine	Sigma-Aldrich	Cat#A2786
Guanine	Sigma-Aldrich	Cat#G11950
Thymine	Sigma-Aldrich	Cat#T0895
Cytosine	Sigma-Aldrich	Cat#C3506
Uracil	Sigma-Aldrich	Cat#U1128
Magnesium sulfate anhydrous	Sigma-Aldrich	Cat#M7506
Manganese(II) sulfate monohydrate	Mallinkrodt	Cat#6192
Sodium chloride	Sigma-Aldrich	Cat#S7653
Iron(II) sulfate heptahydrate	Sigma-Aldrich	Cat#215422
Calcium chloride	Sigma-Aldrich	Cat#C1016
Zinc sulfate heptahydrate	JT Baker Chemical Company	Cat#4382
Copper(II) sulfate pentahydrate	Sigma-Aldrich	Cat#C7631
Boric acid	Sigma-Aldrich	Cat#B6768
Sodium molybdate dehydrate	JT Baker Chemical Company	Cat#3764
Nickel(II) chloride	Sigma-Aldrich	Cat#339350
Alanine	Sigma-Aldrich	Cat#A7469
Arginine	Sigma-Aldrich	Cat#A8094
Asparagine	Sigma-Aldrich	Cat#A4159
Aspartic Acid	Sigma-Aldrich	Cat#A93100
Glutamic Acid	Sigma-Aldrich	Cat#G1501
Glutamine	Sigma-Aldrich	Cat#G8540
Glycine	Thermo Fisher Scientific	Cat#BP381-5
Isoleucine	Sigma-Aldrich	Cat#I2752
Leucine	Sigma-Aldrich	Cat#L8000
Lysine	Sigma-Aldrich	Cat#L5501

(*Continued on next page*)

Continued

REAGENT or RESOURCE	SOURCE	IDENTIFIER
Methionine	Sigma-Aldrich	Cat#M9625
Phenylalanine	Sigma-Aldrich	Cat#P2126
Proline	Sigma-Aldrich	Cat#P5607
Serine	Sigma-Aldrich	Cat#84959
Threonine	Sigma-Aldrich	Cat#T8625
Tyrosine	Sigma-Aldrich	Cat#T3754
Valine	Sigma-Aldrich	Cat#V0500
Tryptone	Thermo Fisher Scientific	Cat#BP1421
Sodium bicarbonate	Sigma-Aldrich	Cat#S5761
Acetic acid	Acros Organics	Cat#222140010
Propionic acid	Acros Organics	Cat#149300010
Isobutyric acid	Alfa Aesar	Cat#79-31-2
Isovaleric acid	Alfa Aesar	Cat#503-74-2
Valeric acid	Alfa Aesar	Cat#109-52-4
Potassium dihydrogen phosphate	Thermo Fisher Scientific	Cat#P284
Dextran sulfate sodium salt (colitis grade, m.w. = 36,000-50,000)	MP Bio	Cat#160110
Critical Commercial Assays		
DNeasy PowerSoil Kit	QIAGEN (formerly Mo Bio)	Cat#12888-100
Nucleospin RNA kit	Macherey-Nagel	Cat#740955.50
SYBR Green PCR Master Mix	Applied Biosystems	Cat#4309155
iScript cDNA Synthesis Kit	Bio-Rad	Cat#1708890
Foxp3 / Transcription Factor Staining Buffer Set	eBioscience	Cat#00-5523-00
Mouse Lipocalin-2/NGAL DuoSet ELISA kit	R&D Systems	Cat#DY1857
Mouse IL-12 p70 DuoSet ELISA kit	R&D Systems	Cat#DY419
Deposited Data		
16S rRNA Sequencing Data	This paper	N/A
Experimental Models: Organisms/Strains		
WT1 mice	Purchased from Jackson Laboratory and bred in the Cancer Center mouse room	N/A
WT2 mice	Derived from mice purchased from Jackson Laboratory and bred in the Cancer Center mouse room	N/A
CD8$^{-/-}$ mice	Purchased from Jackson Laboratory and bred in the Cancer Center mouse room	N/A
GF *Rag1*$^{-/-}$ mice	Germfree facility at UM	N/A
GF WT mice	Germfree facility at UM	N/A
Oligonucleotides		
qPCR primer: Eub F	5′-AGAGTTTGATCCTGGCTC-3′	N/A
qPCR primer: Eub R	5′-TGCTGCCTCCCGTAGGAGT-3′	N/A
qPCR primer: IL-1β F	5′-GATCCACACTCTCCAGCTGCA-3′	N/A
qPCR primer: IL-1β R	5′-CAACCAACAAGTGATATTCTCCATG-3′	N/A
qPCR primer: CXCL9 F	5′-GGAACCCTAGTGATAAGGAATGCA-3′	N/A
qPCR primer: CXCL9 R	3′-TGAGGTCTTTGAGGGATTTGTAGTG-5′	N/A
qPCR primer: CXCL10 F	5′-GACGGTCCGCTGCAACTG-3′	N/A
qPCR primer: CXCL10 R	3′-CTTCCCTATGGCCCTCATTCT-5′	N/A
qPCR primer: IL-6 F	5′-CACATGTTCTCTGGGAAATCG-3′	N/A
qPCR primer: IL-6 R	5′-TTTCTGCAAGTGCATCATCG-3′	N/A
qPCR primer: occludin F	5′-GGGAATGTCCAGAACGAGAAGA-3′	N/A

(*Continued on next page*)

Continued

REAGENT or RESOURCE	SOURCE	IDENTIFIER
qPCR primer: occludin R	5′-CGTGGCAATGAACACCATGA-3′	N/A
qPCR primer: β-defensin2 F	5′-AAGTATTGGATACGAAGCAG-3′	N/A
qPCR primer: β-defensin2 R	5′-TGGCAGAAGGAGGACAAATG-3′	N/A
qPCR primer: Reg3γ F	5′-TCAGGTGCAAGGTGAAGTTG-3′	N/A
qPCR primer: Reg3γ R	5′-GGCCACTGTTACCACTGCTT-3′	N/A
qPCR primer: actin F	5′-CAACTTGATGTATGAAGGCTTTGGT-3′	N/A
qPCR primer: actin R	5′-ACTTTTATTGGTCTCAAGTCAGTGTACAG-3′	N/A
Software and Algorithms		
GraphPad Prism	GraphPad	https://www.graphpad.com/scientific-software/prism/
FlowJo	FlowJo	https://www.flowjo.com/
mothur	Mothur	https://www.mothur.org/
Microsoft Excel	Microsoft	N/A
R	https://www.r-project.org/	N/A
BioRender	https://biorender.com/	N/A

LEAD CONTACT AND MATERIALS AVAILABILITY

Further information and requests for resources and reagents should be directed to and will be fulfilled by the Lead Contact, Grace Chen (gchenry@umich.edu). This study did not generate new unique reagents.

EXPERIMENTAL MODEL AND SUBJECT DETAILS

Animals

SPF WT1 and *Cd8*$^{-/-}$ (B6.129S2-*Cd8a*^{tm1Mak}) mice (all C57BL/6 background) were originally purchased from Jackson Laboratory and bred in-house at the University of Michigan (UM). WT2 mice were generated from WT littermates (*Nod1*$^{+/+}$) of backcrosses between B6/J mice originally purchased from Jackson Laboratory and transgenic *Nod1*$^{-/-}$ mice (> F8) and subsequently established as a separate wild-type colony on a different rack from WT1 to minimize cross-contamination of WT1 and WT2 microbiomes. Adult male or female 6-10 week-old mice were used except in antibiotic experiments where mice began antibiotic treatment at 4-5 weeks old and cohousing experiments which were done with adult females. Cross-fostered WT1 and WT2 pups were switched to a nursing dam of the opposite colony within 48 hours of birth. GF WT and GF *Rag1*$^{-/-}$ mice (all C57BL/6 background, derived from Jackson Laboratory mice) were bred and housed at the UM Germ-free mouse facility. Sterility was regularly verified by aerobic and anaerobic cultures, Gram stains and qPCR. GF mice were conventionalized via oral gavage of cecal and stool contents from either SPF WT1 or WT2 mice. Animal studies were conducted under protocols approved by the University of Michigan Committee on the Use and Care of Animals.

METHOD DETAILS

Inflammation-Induced Colon Tumorigenesis

Age- and sex-matched 6-10 week-old mice were injected intraperitoneally with 10mg azoxymethane (Sigma) per kg mouse weight. After five days, mice were treated with three cycles of 2% dextran sulfate sodium (MP Bio, m.w. = 36,000-50,000) given for five days in the drinking water followed by 16 days of regular drinking water. Depending on the particular experiment, mice were sacrificed between days 60-70 after AOM injection as specified in the Figure. This time range does not significantly affect tumor numbers between mice of the same group (data not shown). For tumor counting, colons were flushed of stool with PBS, longitudinally cut open and grossly counted using a magnifier and measured with calipers. For experiments involving GF and conventionalized GF mice, mice were treated with either 1.5% or 2% depending on the experiment. For example, in Figure 3, all groups were treated with two rounds of 2% and a final round of 1.5% DSS water due to increased mortality of GF+WT2 microbiota after two DSS rounds. In Figures 5B–5D, all groups received three rounds of 1.5% DSS water to ensure 100% survival.

Bacteria Preparation for Oral Gavage

Whole SPF stool and cecal contents were isolated from WT1 and WT2 mice. Specifically, stool and cecal contents were collected under strictly anaerobic conditions (85% N_2, 10% H_2, 5% CO_2) in a Coy anaerobic chamber immediately after euthanasia and homogenized in anaerobic PBS. Homogenates were also plated onto either brain-heart infusion (BHI, BD) agar supplemented with 10%

horse blood (Quad Five), chopped-meat carbohydrate broth (CMCB) agar (Hehemann et al., 2012), or YCFA agar (Ze et al., 2012). Plates were cultured at 37°C anaerobically for 48 hours. Cultivable bacteria were resuspended from plates using anaerobic PBS and gavaged into GF WT mice.

Antibiotic and Antifungal Treatment of Mice

4-5 week old mice were treated with antibiotic and antifungal water for one week to target Gram-positive, Gram-negative and anaerobic bacteria and to prevent fungal blooms (Kennedy et al., 2018). Mice were treated with an antibiotic cocktail consisting of 0.5g/L vancomycin (Pfizer), 2g/L streptomycin (Sigma), 0.75 g/L metronidazole (Sigma), and 0.5g/L fluconazole (Sigma) that was sterile-filtered prior to administration. 2% sucralose (Apriva, Kroger®) was added to increase the antibiotic solution palatability (Abt et al., 2012). Mice then received regular water for 24 hours, gavaged with WT1 or WT2 stool and cecal homogenates for three consecutive days, then AOM/DSS treatment four weeks later.

Isolation of Lamina Propria Cells

Colon LP cells were isolated as previously described (Chen et al., 2008; Zhan et al., 2016). Briefly, whole colons were isolated from naive 6-10 week old WT1 and WT2 mice and cut into small pieces and washed with HBSS (GIBCO) supplemented with 2.5% heat-inactivated FBS (Sigma Aldrich) and penicillin/streptomycin (HBSS+). After two washes with magnetic stirring, colon pieces were incubated in HBSS+ with 1mM DTT (Invitrogen) at 37°C. Colon pieces were washed once and incubated twice in HBSS+ with 1mM EDTA (Lonza) at 37°C with magnetic stirring for 30 minutes. After washing twice, colon tissue was digested in HBSS+ with 400 I.U./mL type III collagenase (Worthington) and 10 μg/mL DNase I (Worthington) at 37°C with magnetic stirring. The single cell suspension was filtered through a 70-micron filter and colon LP immune cells were collected at the interface of a 40%/75% Percoll gradient after centrifugation. For tumor endpoint analyses, tumor or adjacent tissue were cut from the colons and processed as described above but with a single EDTA step.

Flow Cytometry and Intracellular Cytokine Staining

LP cells were isolated from mice at day 0, day 12 of AOM/DSS or at the tumor endpoint (typically day 60). For intracellular staining, cells were incubated for 4 hours at 37°C with 1) GolgiStop (monensin, BD), 100 ng/ml PMA (Sigma) and 1000 ng/ml ionomycin, or 2) with GolgiStop alone ("no stim"). Cells were surface stained, fixed and permeabilized using the Foxp3/Transcription Factor Staining Buffer Set (eBioscience), and then incubated with fluorochrome-conjugated antibodies against PE-Cy7 IFNγ (Biolegend), FITC IL17A (Biolegend), and PE Foxp3 (eBioscience). Samples were analyzed by a BD LSRFortessa, FACSCanto II, or FACSAria II flow cytometer. Foxp3 staining was done on unstimulated cells.

Preparation of Heat-Killed Bacteria

Stool pellets from SPF WT1 and WT2 mice were homogenized in PBS, strained through a 40um cell strainer, and centrifuged at 1000rpm for 10 s to pellet debris. The supernatant was centrifuged at 5000rpm for 10 minutes. The white bacteria layer of the pellet was diluted in PBS and incubated at 95°C for one hour. Heat-killed bacteria suspensions were stored at −20°C until use.

BMDC Preparation and Stimulation

BMDCs were prepared from WT1 and WT2 mice as previously described (Toubai et al., 2019). Briefly, bone marrow cells were cultured for seven days in RPMI (GIBCO) supplemented with 10% FBS (Sigma Aldrich), 1% penicillin/streptomycin, 1% L-glutamine, and 20 ng/ml GM-CSF (Peprotech) (BMDC-media). BMDCs were isolated using the CD11c Microbeads Ultrapure (Miltenyi Biotec) kit. $4x10^5$ BMDCs were cultured with $4x10^6$ heat-killed bacteria for four hours, washed once in PBS, and were resuspended in fresh BMDC-media for another 20 hours.

ELISA (lipocalin-2 and IL-12p70)

Stool was collected on day 0, 12, 26 or 60 of AOM/DSS and homogenized in PBS at 100 mg/ml. Homogenates were diluted to a range of 1:100 to 1:100000 and lcn-2 was measured using the Lcn-2/NGAL ELISA kit (R&D Systems). IL-12p70 was measured in 24 hour supernatants of heat-killed bacteria-stimulated BMDCs (described below) using the IL-12p70 ELISA kit (R&D Systems).

Histologic Scoring

Histological assessment of H&E sections was performed in a blinded fashion by a pathologist (KAE) using a previously described scoring system with modifications (Chen et al., 2008). A point scale was used to denote the severity of inflammation (0 = none, 1 = mild/mucosa only, 2 = moderate infiltration of mucosa/extension to submucosa, 3 = severe in mucosa and submucosa, and 4 = transmural), severity of epithelial loss (0 = none, 1 = mild/basal 1/3 of glands, 2 = moderate/basal 2/3 crypts, 3 = severe where only surface epithelium remains, 4 = ulceration/erosion), and quantification of adenoma/carcinoma (0 = none, 1 = single focus, 2 = multiple foci). Each parameter was multiplied by a factor reflecting the percentage of colon involvement (0%, 25% or less, 26%–50%, 51%–75%, or 76%–100%) and then summed to obtain the overall score.

Isolation of Bacterial DNA and 16S rRNA Sequences Analyses

16S rRNA analysis was performed with fecal samples that had been collected from 6-12 week old mice on the day of AOM injection and were frozen at −20 or −80°C. Bacterial DNA was isolated using the PowerSoil-htp 96 Well Soil DNA isolation kit (QIAGEN) with the epMotion 5075 or manually with the DNeasy PowerSoil Kit (QIAGEN). The V4 region of the 16S rRNA gene was amplified using custom barcoded primers, sequenced with the Illumina MiSeq Personal Sequencing platform, and processed using the mothur software package to reduce sequencing errors and remove chimeras as previously described (Kozich et al., 2013; Schloss et al., 2009). Sequences were aligned to the SILVA 16S rRNA sequence database (Pruesse et al., 2007). Sequences were clustered into operational taxonomic units (OTUs) using a 97% similarity cutoff. Parallel sequencing and processing of a mock community allowed us to determine a sequencing error rate of 1.38%. Dissimilarity in community structure between samples was calculated using the θ_{YC} (thetaYC) distance metric. ThetaYC distances between samples were used for two-dimensional ordination analysis by non-metric dimensional scaling (NMDS). Microbial alpha diversity was calculated using the inverse Simpson index and the observed number of OTUs (richness) (Zackular et al., 2013). Analysis of molecular variance (AMOVA) was used to determine significance between community structure differences of different groups of samples. A random forest regression model (see Statistical Analysis) was used to identify OTUs that are associated with the number of tumors on the day of AOM injection (Zackular et al., 2015). Linear and Poisson regression analyses were used to correlate OTUs to tumor burdens. OTUs identified to be predictive of tumor outcomes based on random forest (see Statistical Analysis) and regression models were cross-referenced with LEfSe and Metastats methods, which were used to identify OTUs associated with low (0-5 tumors) or high (> 15) tumor burdens based on abundance, using an LDA score cutoff of 3 and an abundance difference cutoff of 0.003, respectively. OTUs that were significant in all five statistical models were chosen as candidates. A phylogenetic tree of the candidates was generated based on the V4 region sequence of the 16S rRNA gene using the Clustal Omega program by the EMBL-EBI (Madeira et al., 2019).

RNA Isolation and qPCR

Intraepithelial cells were isolated from untreated WT1 and WT2 mice from the EDTA steps of LP immune cell isolation. Total RNA was isolated using the Nucleospin RNA kit (Macherey-Nagel). cDNA synthesis was performed using the iScript cDNA synthesis kit (BioRad) and used for quantitative PCR using SYBR Green on the ABI 7900HT. Gene transcript levels were normalized to actin. Primer sequences can be found in the Key Resources Table.

Graphics

Graphical Abstract was created with BioRender.com

QUANTIFICATION AND STATISTICAL ANALYSIS

Continuous data are shown as mean ± SEM. Sample sizes can be found in the Figure Legends. Statistical analyses were performed using GraphPad Prism7, R and mothur software. Statistically significant differences were determined by Mann-Whitney when only two groups are compared (e.g., tumor numbers, fecal Lcn-2 levels). Differences in bacterial community structure were analyzed using AMOVA in mothur (Excoffier et al., 1992). P values below 0.05 were considered statistically significant and are represented as follows: * $p < 0.05$. A random forest (RF) regression model was used to identify OTUs that are associated with the number of tumors that developed. RF is a decision tree-based approach that allows for nonlinear relationship between the OTU and tumor count data and interactions between OTUs. The RF model included all 521 OTUs with a total normalized count over all mice > 0.005. It was fit using the randomForest package in R with *default parameters* except that we increased the number of trees in RF to 1,000 trees (Breiman, 2001). Finally, OTUs were ranked by importance in the RF model as determined by the percent reduction in the mean square error (MSE) when an OTU was removed from the model. As an alternative to the machine learning method, we also used parametric regression models to study the effect of each OTU on the tumor count data. Specifically, we considered the simple linear regression (lm function in R) and Poisson regression (glm function in R). The resulting p values were adjusted to control the false discovery rate (Benjamini and Yekutieli, 2001).

DATA AND CODE AVAILABILITY

The accession number for the FASTQ sequences reported in this paper is Sequence Read Archive: PRJNA557261.

Cell Reports, Volume *31*

Supplemental Information

Gut Microbiota Modulate CD8 T Cell Responses to Influence Colitis-Associated Tumorigenesis

Amy I. Yu, Lili Zhao, Kathryn A. Eaton, Sharon Ho, Jiachen Chen, Sara Poe, James Becker, Allison Gonzalez, Delaney McKinstry, Muneer Hasso, Jonny Mendoza-Castrejon, Joel Whitfield, Charles Koumpouras, Patrick D. Schloss, Eric C. Martens, and Grace Y. Chen

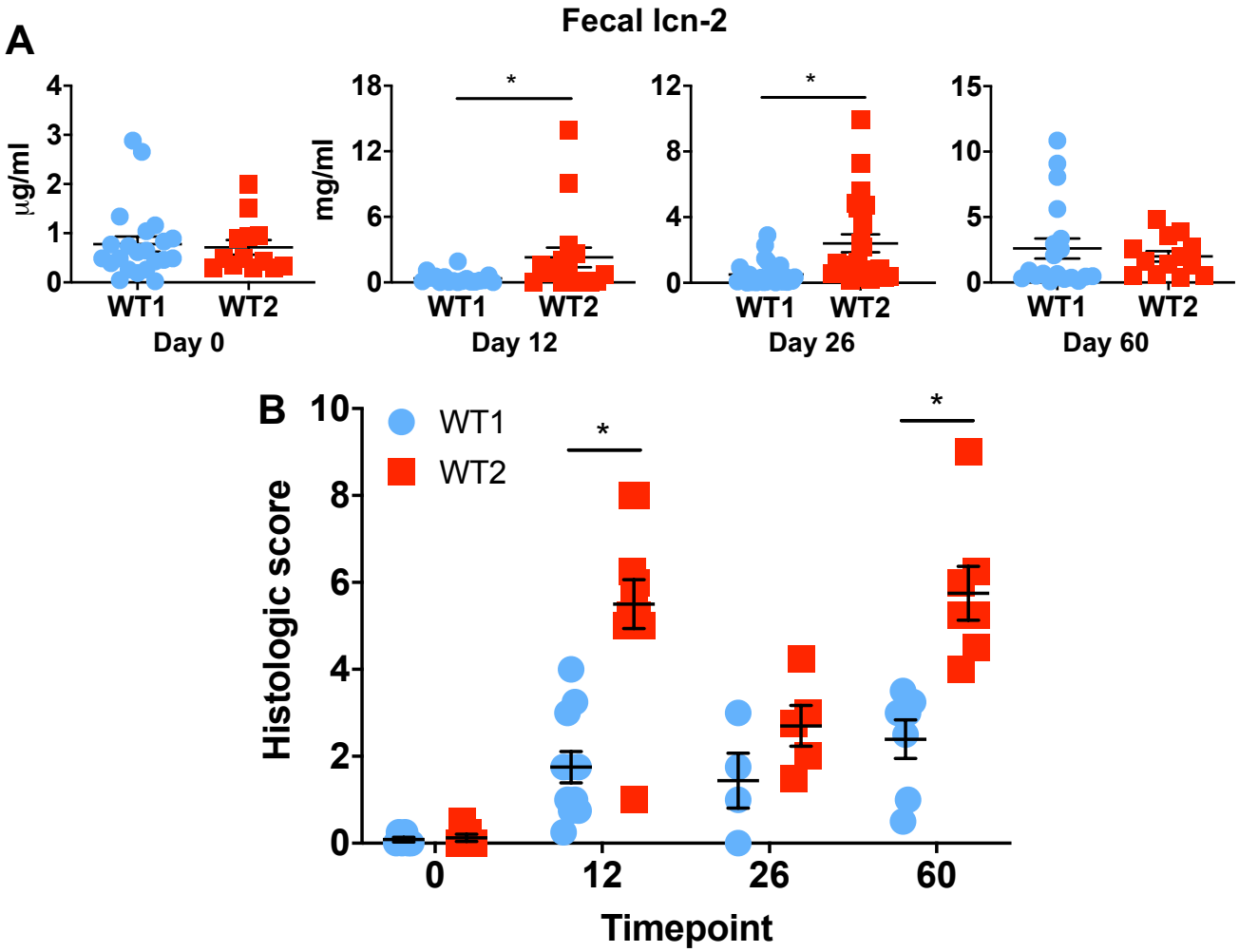

Figure S1. WT2 mice have increased inflammation during AOM/DSS treatment. Related to Figure 1.

(A) Stool lipocalin-2 levels were measured by ELISA on days 0, 12, 26, and 60 of AOM/DSS treatment. D0: WT1 n=22 and WT2 n=13, D12: WT1 n=18 and WT2 n=17, D26: WT1 n=29 and WT2 n=23, D60: WT1 n=19 and WT2 n=13

(B) Severity and extent of inflammatory cell infiltration, epithelial loss and dysplasia of WT1 and WT2 mice on days 0, 12, 26, and 60 of AOM/DSS treatment were assessed by histological scoring. D0: n=6/group, D12: n=11/group, D26: WT1 n=4 and WT2 n=5, D60: n=7/group

Data are mean ± SEM. *p<0.05 by Mann-Whitney

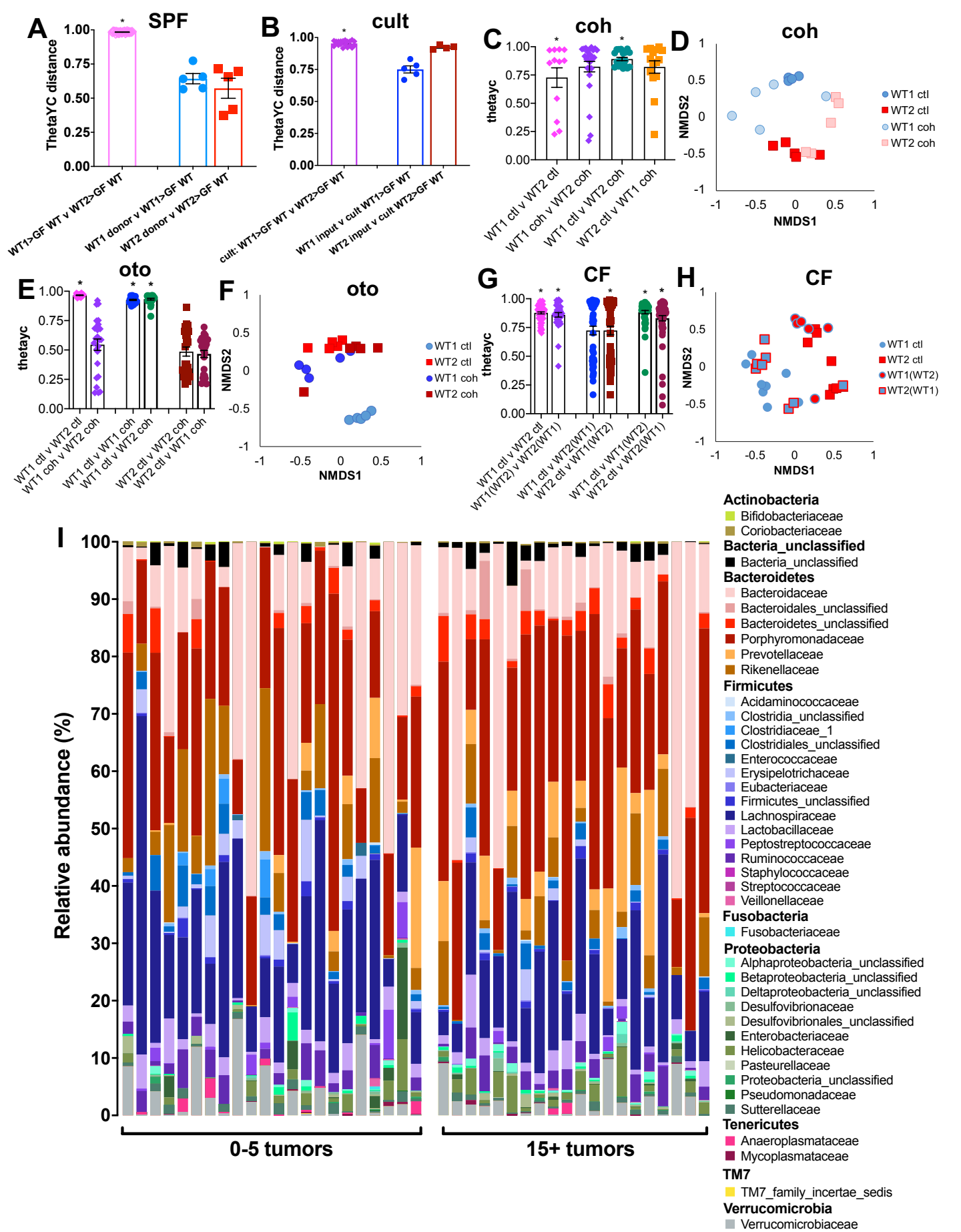
A
SPF
ThetaYC distance
WT1>GF WT v WT2>GF WT
WT1 donor v WT1>GF WT
WT2 donor v WT2>GF WT
B
cult
ThetaYC distance
cult: WT1>GF WT v WT2>GF WT
WT1 input v cult WT1>GF WT
WT2 input v cult WT2>GF WT
C
coh
thetayc
WT1 ctl v WT2 ctl
WT1 coh v WT2 coh
WT1 ctl v WT2 coh
WT2 ctl v WT1 coh
D
coh
NMDS2
NMDS1
WT1 ctl
WT2 ctl
WT1 coh
WT2 coh
E
oto
thetayc
WT1 ctl v WT2 ctl
WT1 coh v WT2 coh
WT1 ctl v WT1 coh
WT1 ctl v WT2 coh
WT2 ctl v WT2 coh
WT2 ctl v WT1 coh
F
oto
NMDS2
NMDS1
WT1 ctl
WT2 ctl
WT1 coh
WT2 coh
G
CF
thetayc
WT1 ctl v WT2 ctl
WT1(WT2) v WT2(WT1)
WT1 ctl v WT2(WT1)
WT2 ctl v WT1(WT2)
WT1 ctl v WT1(WT2)
WT2 ctl v WT2(WT1)
H
CF
NMDS2
NMDS1
WT1 ctl
WT2 ctl
WT1(WT2)
WT2(WT1)
I
Relative abundance (%)
0-5 tumors
15+ tumors
Actinobacteria
Bifidobacteriaceae
Coriobacteriaceae
Bacteria_unclassified
Bacteria_unclassified
Bacteroidetes
Bacteroidaceae
Bacteroidales_unclassified
Bacteroidetes_unclassified
Porphyromonadaceae
Prevotellaceae
Rikenellaceae
Firmicutes
Acidaminococcaceae
Clostridia_unclassified
Clostridiaceae_1
Clostridiales_unclassified
Enterococcaceae
Erysipelotrichaceae
Eubacteriaceae
Firmicutes_unclassified
Lachnospiraceae
Lactobacillaceae
Peptostreptococcaceae
Ruminococcaceae
Staphylococcaceae
Streptococcaceae
Veillonellaceae
Fusobacteria
Fusobacteriaceae
Proteobacteria
Alphaproteobacteria_unclassified
Betaproteobacteria_unclassified
Deltaproteobacteria_unclassified
Desulfovibrionaceae
Desulfovibrionales_unclassified
Enterobacteriaceae
Helicobacteraceae
Pasteurellaceae
Proteobacteria_unclassified
Pseudomonadaceae
Sutterellaceae
Tenericutes
Anaeroplasmataceae
Mycoplasmataceae
TM7
TM7_family_incertae_sedis
Verrucomicrobia
Verrucomicrobiaceae

Figure S2

Figure S2. Microbiome colonization after microbiome transfer experiments. Related to Figures 3 and 4.

(A and B) Microbiome composition similarity of GF WT mice colonized with whole SPF stool and cecal contents **(A)** or cultivable bacteria **(B)** of WT1 or WT2 mice was analyzed by ThetaYC distance between groups.

(C and D) WT1 and WT2 mice were cohoused (2:2) and stool was collected after four weeks for microbiome analysis. **(C)** Microbiome composition dissimilarity was analyzed by ThetaYC distance. **(D)** Beta diversity is shown as a non-metric dimensional scaling plot (NMDS).

(E and F) WT1 and WT2 mice were cohoused (1:1) and stool was collected after six weeks for microbiome analysis. Microbiome composition dissimilarity was analyzed by ThetaYC distance **(E)** and shown as an NMDS plot **(F)**.

(G and H) WT1 and WT2 mice were cross-fostered and stool was collected from 6-week-old mice for microbiome analysis. Microbiome composition dissimilarity was analyzed by ThetaYC distance **(G)** and shown as an NMDS plot **(H)**.

(I) Stool was collected on day 0 before AOM injection. Relative abundances of family-level bacteria in naive mice that eventually developed low (0-5) or high (15+) tumors after AOM/DSS treatment are shown. Low tumor n=22, high tumor n=20

Data are representative of or pooled from at least two independent experiments. *$p<0.05$ by AMOVA

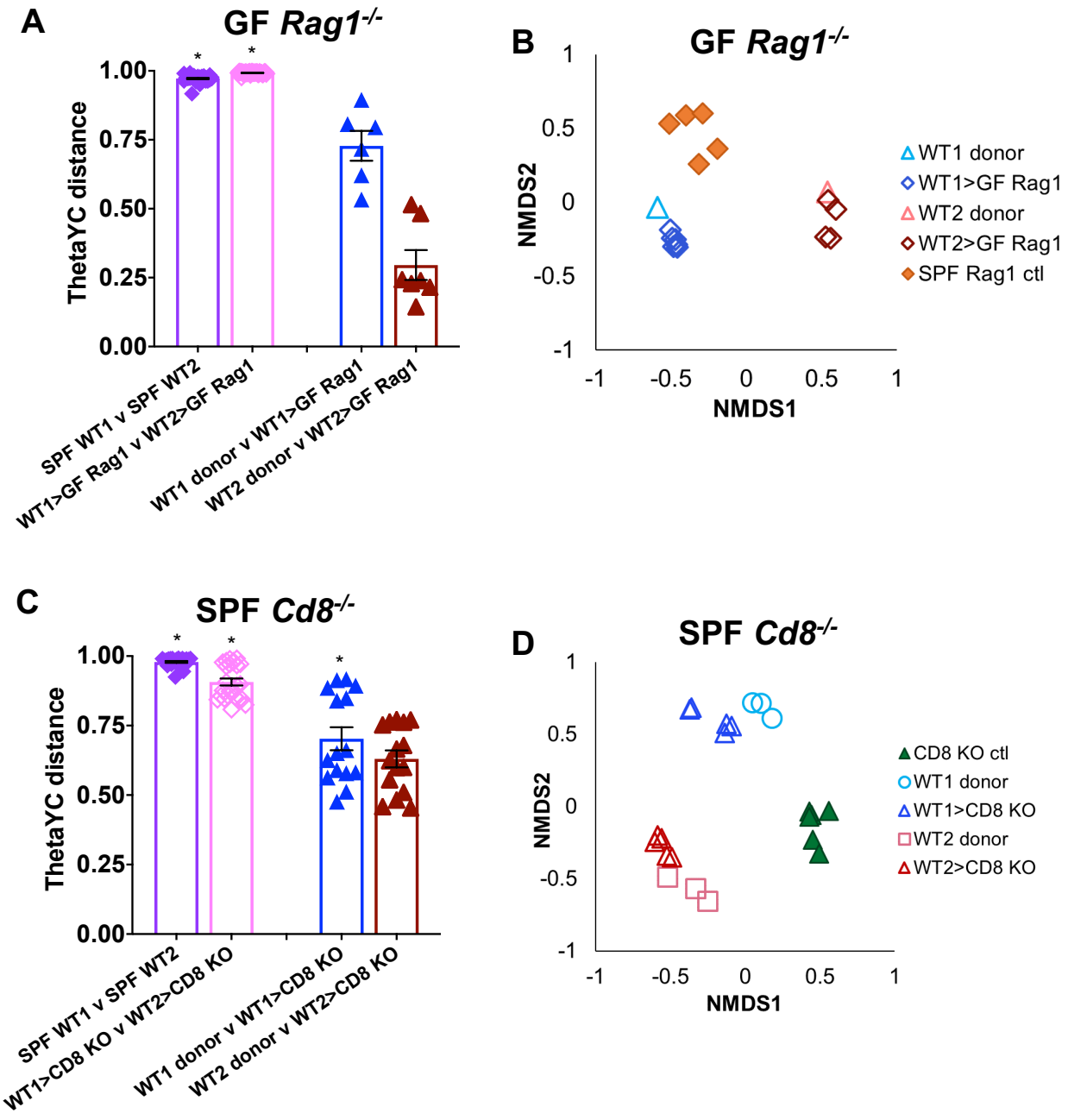

Figure S3. Beta diversity of GF *Rag1*$^{-/-}$ or SPF *Cd8*$^{-/-}$ mice colonized with SPF WT1 or WT2 microbiomes. Related to Figures 5 and 6.

(A and B) 16S rRNA sequencing of fecal microbiota of naïve mice was used to assess microbiome differences between GF *Rag1*$^{-/-}$ mice colonized with SPF WT1 or WT2 stool homogenates. Microbiome composition dissimilarity was analyzed by ThetaYC distance **(A)** and shown as an NMDS plot **(B)**.

(C and D) 16S rRNA sequencing of fecal microbiota of naïve mice was used to assess microbiome differences between SPF *Cd8*$^{-/-}$ mice recolonized with SPF WT1 or WT2 stool homogenates after antibiotic and antifungal treatment. Microbiome composition dissimilarity was analyzed by ThetaYC distance **(C)** and shown as an NMDS plot **(D)**.

n=4-6/group, *p<0.05 by AMOVA

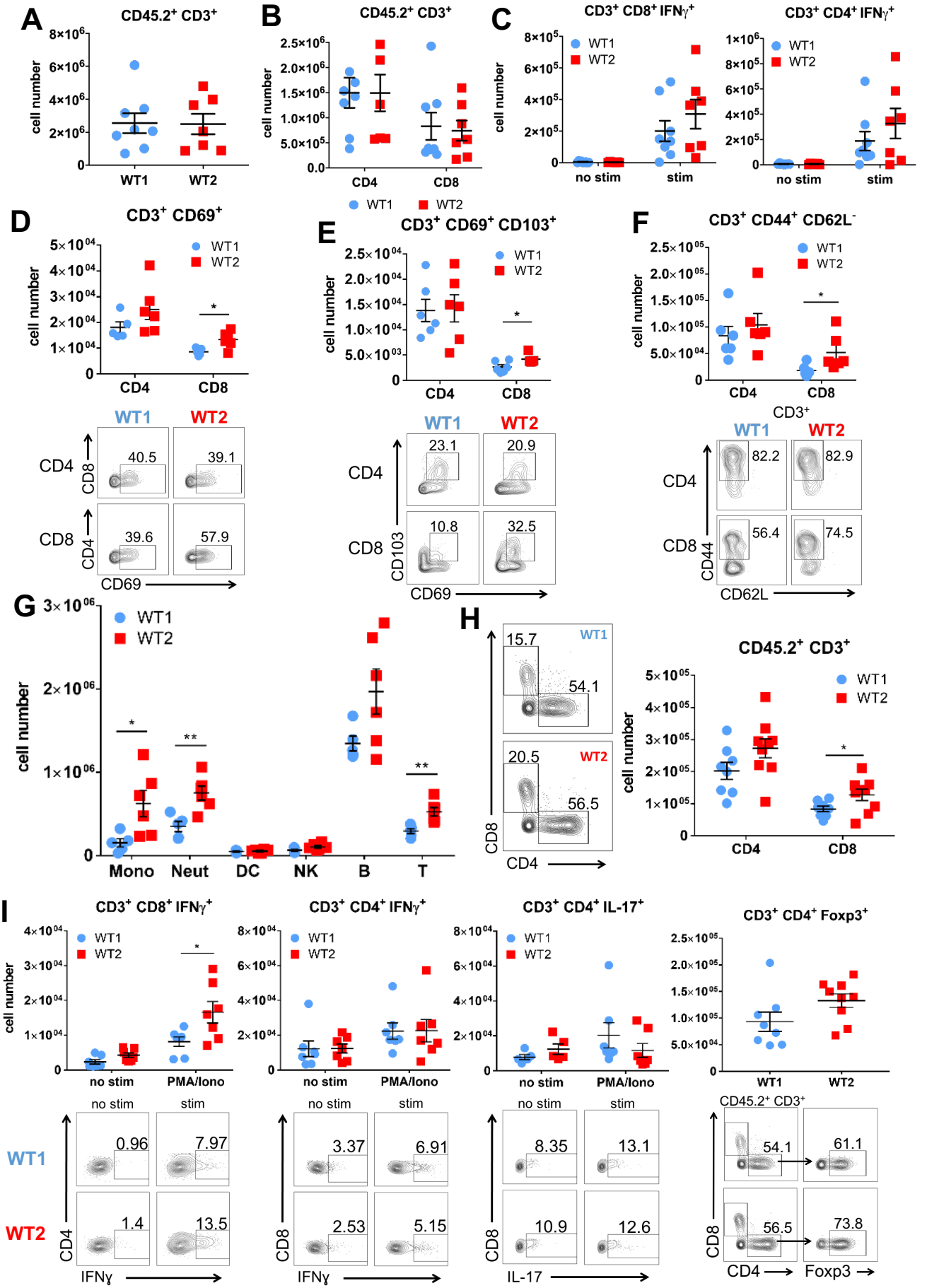
A
CD45.2+ CD3+
cell number
WT1
WT2
B
CD45.2+ CD3+
CD4
CD8
C
CD3+ CD8+ IFNγ+
CD3+ CD4+ IFNγ+
no stim
stim
D
CD3+ CD69+
E
CD3+ CD69+ CD103+
F
CD3+ CD44+ CD62L-
CD3+
40.5
39.1
39.6
57.9
23.1
20.9
10.8
32.5
82.2
82.9
56.4
74.5
CD69
CD103
CD44
CD62L
G
Mono
Neut
DC
NK
B
T
H
15.7
54.1
20.5
56.5
I
PMA/Iono
IFNγ
IL-17
Foxp3
0.96
7.97
1.4
13.5
3.37
6.91
2.53
5.15
8.35
13.1
10.9
12.6
54.1
61.1
56.5
73.8

Figure S4

Figure S4. Naive WT2 mice have increased activated and effector memory colon lamina propria CD8 T cells and no T cell differences in the mesenteric lymph nodes. Colon lamina propria $CD8^+$ $IFN\gamma^+$ T cells are increased in WT2 mice on day 12 of AOM/DSS treatment. Related to Figure 6.

(A-C) Mesenteric lymph node (MLN) cells from untreated WT1 and WT2 mice were *ex vivo*-stimulated. T cell subsets **(A and B)** and IFNɣ activity **(C)** were analyzed by flow cytometry.

(D-F) Naive colon LP T cells were analyzed for activation **(D)**, resident memory T cells **(E)**, and T memory subsets **(F)**. Cells are gated on $CD45.2^+$ $CD3^+$ or $CD3^+$.

(G and H) Mice were injected with AOM and five days later, treated with 2% DSS for five days. Two days after DSS treatment completion, mice were sacrificed for colon LP flow cytometry analysis. Colon LP immune cells **(G)** and T cell subsets **(H)** were analyzed by flow cytometry.

(I) Colon lamina propria immune cells were *ex vivo*-stimulated with PMA and ionomycin and monensin for four hours before flow cytometry analysis. Non-stimulated cells were incubated with monensin for four hours before and flow cytometry analysis.

Data are mean ± SEM and are pooled from at least two independent experiments. n=5-9/group. *$p<0.05$ by Mann-Whitney

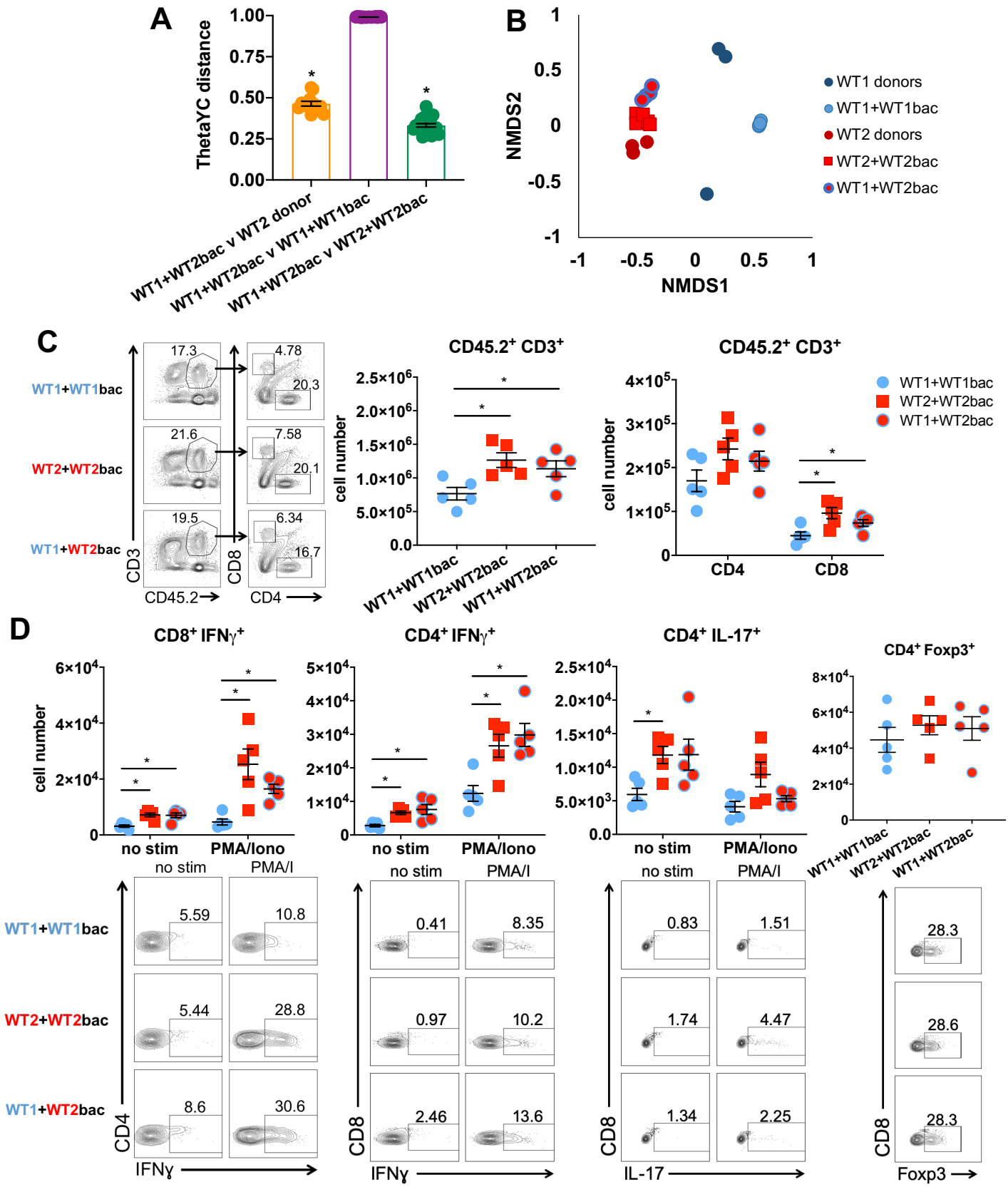
A
ThetaYC distance
1.00
0.75
0.50
0.25
0.00
WT1+WT2bac v WT2 donor
WT1+WT2bac v WT1+WT1bac
WT1+WT2bac v WT2+WT2bac
B
NMDS2
NMDS1
WT1 donors
WT1+WT1bac
WT2 donors
WT2+WT2bac
WT1+WT2bac
C
WT1+WT1bac
WT2+WT2bac
WT1+WT2bac
CD3
CD8
CD45.2
CD4
17.3
4.78
20.3
21.6
7.58
20.1
19.5
6.34
16.7
CD45.2+ CD3+
cell number
WT1+WT1bac
WT2+WT2bac
WT1+WT2bac
CD4
CD8
D
CD8+ IFNγ+
CD4+ IFNγ+
CD4+ IL-17+
CD4+ Foxp3+
cell number
no stim
PMA/Iono
PMA/I
5.59
10.8
5.44
28.8
8.6
30.6
0.41
8.35
0.97
10.2
2.46
13.6
0.83
1.51
1.74
4.47
1.34
2.25
28.3
28.6
28.3
IFNγ
IL-17
Foxp3

Figure S5

Figure S5. SPF WT1 mice colonized with WT2 microbiota develop increased colon lamina propria $CD8^+$ $IFN\gamma^+$ T cells. Related to Figure 6.

SPF WT1 and WT2 mice were treated with antibiotics and antifungal water for one week prior to three consecutive gavages of SPF WT1 or WT2 microbiota. Nine weeks after colonization, the colon LP was analyzed by flow cytometry.

(A and B) Microbiome composition dissimilarity was analyzed by ThetaYC distance **(A)** and shown as an NMDS plot **(B)**. *p<0.05 by AMOVA

(C) CD3 T cell and T cell subsets were analyzed by flow cytometry.

(D) Colon lamina propria immune cells were *ex vivo*-stimulated with PMA and ionomycin and monensin for four hours before flow cytometry analysis. Non-stimulated cells were incubated with monensin for four hours before and flow cytometry analysis.

Data are mean ± SEM and are representative of two independent experiments. n=5/group, *p<0.05 by Mann-Whitney unless otherwise noted

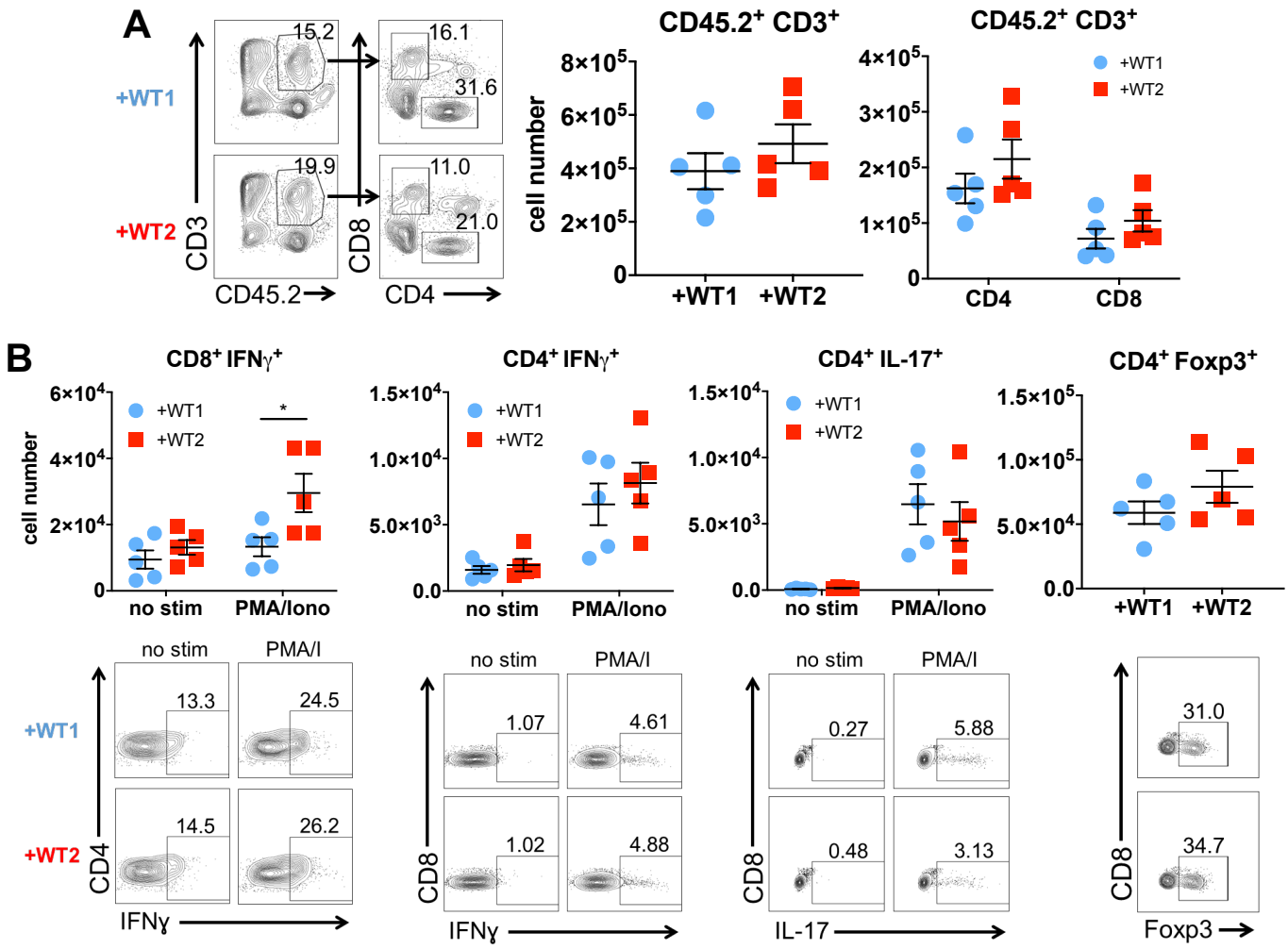

Figure S6. GF WT mice colonized with WT2 microbiota develop increased colon lamina propria CD8⁺ IFNγ⁺ T cells. Related to Figure 6.

GF WT mice were gavaged with SPF WT1 or WT2 microbiota. Eight weeks after colonization, the colon LP was analyzed by flow cytometry.

(A) CD3 T cell and T cell subsets were analyzed by flow cytometry.

(B) Colon lamina propria immune cells were *ex vivo*-stimulated with PMA and ionomycin and monensin for four hours before flow cytometry analysis. Non-stimulated cells were incubated with monensin for four hours before and flow cytometry analysis.

Data are mean ± SEM. n=5/group, *p<0.05 by Mann-Whitney

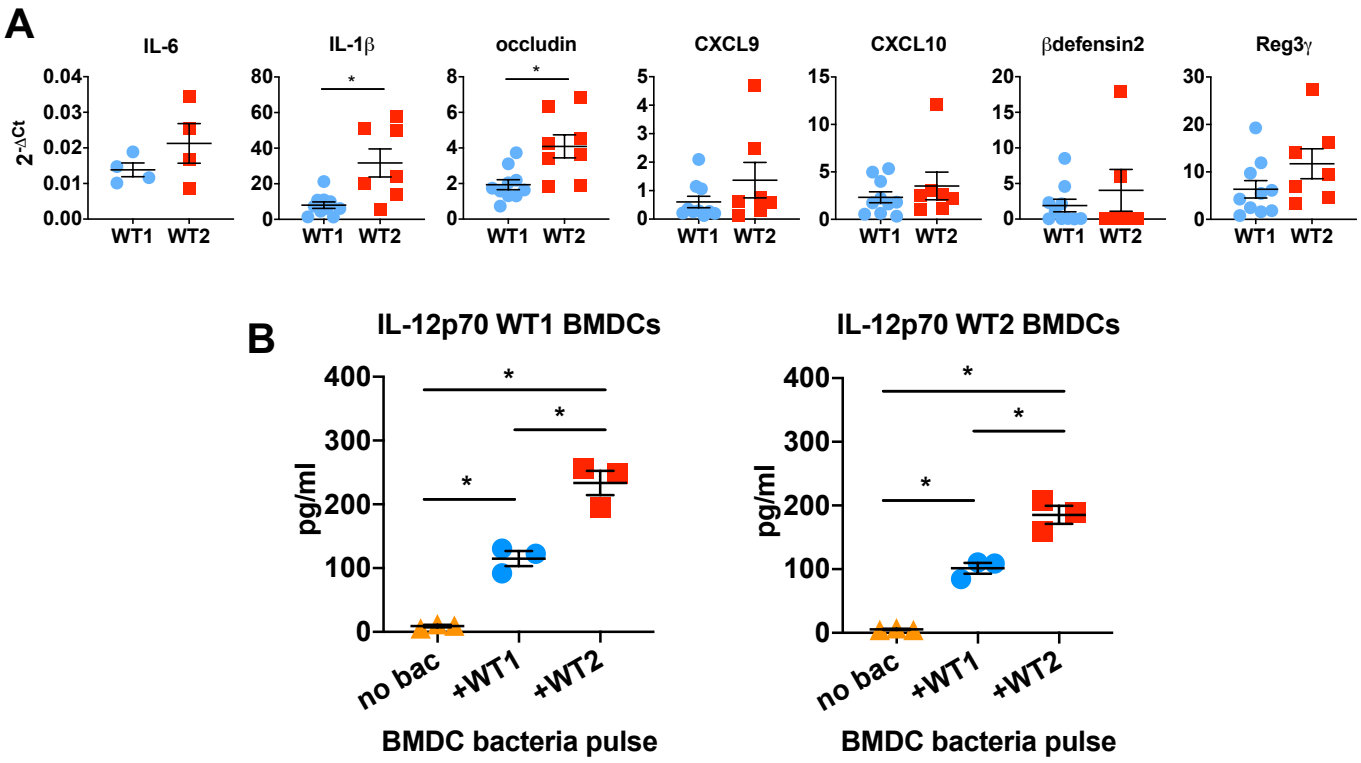

Figure S7. WT2 microbiota results in increased production of IL-12 production by BMDCs. Related to Figure 6.

(A) mRNA expression of several epithelial cell-related genes relative to actin by untreated WT1 and WT2 epithelial cells. IL-6: n=4/group; rest: WT1 n=10, WT2 n=6 (βdef2), 7 (CXCL9, Reg3ɣ, and IL-1β), or 8 (CXCL10 and occludin). *p<0.05 by Mann-Whitney

(B) IL-12p70 levels were measured by ELISA in 24-hour supernatants of bone marrow-derived dendritic cells exposed to heat-killed SPF WT1 or WT2 bacteria cultures. n=3 mice/colony. WT1 data are representative of three independent experiments. WT2 data are representative of two independent experiments. *p<0.05 by Mann-Whitney